

# 1 Influence of meteorology and anthropogenic pollu- 2 tion on chemical flux divergence of the NO-NO<sub>2</sub>-O<sub>3</sub> 3 triad above and within a natural grassland canopy

4 D. Plake<sup>1</sup>, M. Sörgel<sup>1</sup>, P. Stella<sup>1\*</sup>, A. Held<sup>2</sup> and I. Trebs<sup>1\*\*#</sup>

5

6 [1] *Max Planck Institute for Chemistry, Biogeochemistry Department, P. O. Box 3060, 55020*  
7 *Mainz, Germany.*

8 [2] *University of Bayreuth, Junior Professorship in Atmospheric Chemistry, Bayreuth, Ger-*  
9 *many.*

10 \* *now at: AgroParisTech, UMR INRA/ AgroParisTech SAD-APT, Paris, France*

11 \*\* *now at: ~~Centre de Recherche Public – Gabriel Lippmann, Department Environment and~~*  
12 *~~Agro-biotechnologies, 41 rue du Brill, L-4422 Belvaux, Luxembourg~~ Luxembourg Institute of*  
13 *Science and Technology, Environmental Research and Innovation (ERIN) Department, 5 ave-*  
14 *nue des Hauts-Fourneaux, L-4362 Esch/Alzette, Luxembourg*

15 *Corresponding author: [ivonne.trebs@list.lu](mailto:ivonne.trebs@list.lu)*

16

17

## 18 Abstract

19 The detailed understanding of surface-atmosphere exchange fluxes of reactive trace gases  
20 species is a crucial precondition for reliable modeling of processes in atmospheric chemistry.  
21 Plant canopies significantly impact the atmospheric budget of trace gases. In the past, many  
22 studies focused on taller forest canopies or crops, where the bulk plant material is concentrat-

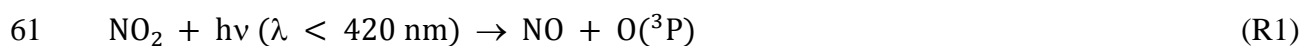
23 ed in the uppermost canopy layer. However, within grasslands, a land-cover class that global-  
24 ly covers vast terrestrial areas, the canopy structure is fundamentally different, as the main  
25 biomass is concentrated in the lowest part of the canopy ~~part~~. This has obvious implications  
26 for aerodynamic in-canopy transport, and consequently also impacts on global budgets of key  
27 species in atmospheric chemistry such as nitric oxide (NO), nitrogen dioxide (NO<sub>2</sub>) and ozone  
28 (O<sub>3</sub>).

29 This study presents for the first time a comprehensive data set of directly measured in-canopy  
30 transport times and aerodynamic resistances, chemical timescales, Damköhler numbers, trace  
31 gas and micrometeorological measurements for a natural grassland canopy (canopy height =  
32 0.6 m). Special attention is paid to the impact of contrasting meteorological and air chemical  
33 conditions on in-canopy transport and chemical flux divergence. Our results show that the  
34 grassland canopy is decoupled throughout the day. In the lower most canopy layer, the meas-  
35 ured transport times are fastest during nighttime, which is due to convection during nighttime  
36 and a stable stratification during daytime in this layer. The inverse was found in the layers  
37 above. During periods of low wind speed and high NO<sub>x</sub> (NO+NO<sub>2</sub>) levels, the effect of cano-  
38 py decoupling on trace gas transport was found to be especially distinct. The aerodynamic  
39 resistance in the lower most canopy layer (0.04–0.2 m) was around 1000 s m<sup>-1</sup>, ~~thus which is~~  
40 as high as values ~~from literature representing determined previously for~~ the lowest meter of an  
41 Amazonian rain forest canopy. The aerodynamic resistance representing the bulk canopy was  
42 found to be more than 3–4 times higher as than in forests. Calculated Damköhler numbers  
43 (ratio of transport and chemical timescales) suggested a strong flux divergence for the NO-  
44 NO<sub>2</sub>-O<sub>3</sub> triad within the canopy during daytime. ~~At~~ During that time, the timescale of NO<sub>2</sub>  
45 ~~plant~~ uptake by plants ranged from 90 to 160 s and was the fastest relevant timescale, i.e. fast-  
46 er than the reaction of NO and O<sub>3</sub>. Thus, our results ~~clearly~~ reveal that grassland canopies of

47 similar structure ~~have exhibit~~ a strong potential to retain soil emitted NO ~~by due to oxidation~~  
48 ~~and subsequent~~ uptake of NO<sub>2</sub> by ~~the~~ plants. Furthermore, ~~a~~ photo-chemical O<sub>3</sub> production  
49 ~~was observed~~ above the canopy ~~was observed~~, ~~which was attributed to a deviation from the~~  
50 ~~NO-NO<sub>2</sub>-O<sub>3</sub> photostationary state by a surplus of NO<sub>2</sub> due to oxidation of NO by e.g., peroxy~~  
51 ~~radicals. which resulted from a surplus of NO<sub>2</sub> from the NO-NO<sub>2</sub>-O<sub>3</sub> photostationary state.~~  
52 The O<sub>3</sub> production was one order of magnitude higher during high NO<sub>x</sub> than during low NO<sub>x</sub>  
53 periods and resulted in an ~~underestimation of the~~ O<sub>3</sub> ~~deposition~~ flux ~~measured with the EC~~  
54 ~~method underestimation, which was observed for the first time.~~

## 55 1 Introduction

56 Nitric oxide (NO) and nitrogen dioxide (NO<sub>2</sub>) play a crucial role in air chemistry ~~since as~~ they  
57 act as key catalysts for ozone (O<sub>3</sub>) production and are therefore involved in the generation of  
58 hydroxyl radicals (OH) (Crutzen, 1973). The most significant tropospheric source of O<sub>3</sub> is  
59 initiated by photochemical dissociation of NO<sub>2</sub> and subsequent reaction of the oxygen (O)  
60 atom with molecular oxygen:



63 ~~When-In case~~ O<sub>3</sub> is present, it may oxidize NO and re-form NO<sub>2</sub>:



65 In the absence of additional reactions, R1–R3 represent a null cycle. Besides R1–R3, NO is  
66 oxidized by peroxy radicals (~~HO<sub>2</sub>+RO<sub>2</sub>~~), ~~which onstituting constitutes~~ an ~~additional~~ important  
67 net O<sub>3</sub> production pathway in the troposphere (Warneck, 2000).

68 Dry deposition to terrestrial surfaces, especially to plant canopies, is an important sink for  
69 tropospheric O<sub>3</sub> and NO<sub>2</sub>. The uncertainties of dry deposition estimates are substantially high-  
70 er for NO<sub>2</sub>, because its net ecosystem exchange can be bi-directional depending on the ambi-  
71 ent NO<sub>2</sub> levels (Lerdau et al., 2000). O<sub>3</sub> instead is exclusively deposited to surfaces. In con-  
72 trast, NO is known to be mainly net emitted from nearly all soil types. Biogenic NO soil  
73 emissions contribute about 20 % to the global NO<sub>x</sub> (NO+NO<sub>2</sub>) emissions (~~IPPC, 2007~~IPPC,  
74 2013), highlighting the need of ~~careful~~detailed investigations on NO<sub>x</sub> soil-atmosphere ex-  
75 change.

76 A major challenge for studies investigating surface-atmosphere exchange fluxes of these reac-  
77 tive trace gases is the presence of plant canopies. These significantly modify the turbulent  
78 properties of the surface and, thus, alter trace gas exchange fluxes. Most previous studies fo-  
79 cused on taller canopies such as forests. However, grassland canopies represent a highly im-  
80 portant land cover class covering globally 41 % and Europe-wide 19 % of the terrestrial land  
81 surface (Suttie et al., 2005; Kasanko et al., 2011). In contrast to forests, grasslands feature the  
82 main bulk plant area density near the soil (e.g., Ripley and Redman, 1976; Jäggi et al., 2006),  
83 accompanied with mean distances between plant elements of only some millimeters (Aylor et  
84 al., 1993). Organized coherent structures govern turbulence dynamics within and above plant  
85 canopies (Finnigan, 2000). The mean in-canopy transport is slower than above the canopy  
86 (e.g., Nemitz et al., 2009). This modification of in-canopy transport has important implica-  
87 tions for global atmospheric chemistry. Plant canopies and the soil below are biologically  
88 actively emitting and taking up reactive trace gases, and ~~they~~conditions within canopies may  
89 provide sufficient time for fast chemical reactions ~~to occur within the canopy~~ (Nemitz et al.,  
90 2009). Subsequently, they modify surface exchange fluxes (e.g., Rinne et al., 2012). For in-  
91 stance, ammonia can be released by a part of the canopy and taken up by another (Nemitz et

92 al., 2000; Denmead et al., 2007). In addition, recapturing of NO<sub>2</sub> originating from biogenic  
93 soil NO emissions after reaction with O<sub>3</sub> within plant canopies (Rummel et al., 2002) is ac-  
94 counted for in global models by a so-called canopy reduction factor for NO<sub>x</sub> (Yienger and  
95 Levy, 1995). However, these estimates are based on only one single experiment in an Ama-  
96 zonian rain forest (Bakwin et al., 1990), and a subsequent model analysis (Jacob and Wofsy,  
97 1990). Canopy reduction for grasslands and other ecosystems was not experimentally studied  
98 up to now. ~~Consequently,~~ The contrasting canopy structure of grassland and forest ecosys-  
99 tems highlights the need for a detailed analysis and an evaluation of the suggested NO<sub>x</sub> cano-  
100 py reduction factor of e.g. 64 % ~~suggested~~ by Yienger and Levy (1995) for temperate grass-  
101 land.

102 Net ecosystem exchange fluxes are typically measured at a certain height above the canopy.  
103 They rely on the constant flux layer assumption (e.g., Swinbank, 1968), which however, may  
104 be violated for reactive trace gases within or just above the vegetation. To assess the potential  
105 chemical divergence of exchange fluxes, the Damköhler number (*DA*) has commonly been  
106 applied (e.g., Rinne et al., 2012). *DA* is calculated as the ratio of the transport time ( $\tau_{tr}$ ) and  
107 the characteristic chemical timescale ( $\tau_{ch}$ ):

$$108 \quad DA = \frac{\tau_{tr}}{\tau_{ch}} \quad (1)$$

109 Hence, *DA* above unity indicates that chemical reactions occur significantly faster than the  
110 transport (flux divergence), whereas *DA* smaller than 0.1 indicate the reverse case. The range  
111 in-between is commonly addressed as a critical range, where an impact of chemistry cannot  
112 be excluded (Stella et al., 2013).

113 In this paper, we present directly measured transport times, chemical timescales and corre-  
114 sponding Damköhler numbers for three layers above and within a natural grassland canopy

115 under contrasting meteorological and air chemical conditions. For the first time, such a com-  
116 prehensive analysis involving trace gas and micrometeorological measurements is made for a  
117 grassland canopy. Furthermore, the consequences of in-canopy processes for NO<sub>x</sub> canopy  
118 reduction and simultaneously measured O<sub>3</sub> deposition fluxes will be discussed.

## 119 2 Material and Methods

### 120 2.1 Site description

121 We performed an intensive field experiment from July to September 2011 at the estate of the  
122 Mainz-Finthen Airport in Rhineland-Palatinate, Germany (further details given in Plake and  
123 Trebs, 2013; Plake et al., 2014; Moravek et al., 2014a). The vegetation at the site was nutri-  
124 ent-poor grassland with a mean canopy height ( $h_c$ ) of 0.6 m and a leaf area index ( $LAI$ ) of 4.8  
125 m<sup>2</sup> m<sup>-2</sup>. A list of species and an  $LAI$  profile are given in Plake et al. (2014), with the latter  
126 indicating a high biomass density below 0.2 m corresponding to 85 % of the total  $LAI$ . Topo-  
127 graphically located on a plateau 150 m above the Rhine valley, the site ~~was is situated located~~  
128 about 9 km south-west of the city center of Mainz. The site was surrounded by villages and  
129 motorways in a distance of 2 to 6 km and 4 to 15 km, respectively. The surrounding area was  
130 mainly characterized by agricultural use for vineyards, orchards and crops. The fetch was  
131 largest in south-western direction without significant anthropogenic pollution sources.

### 132 2.2 Experimental setup

133 A vertical Thoron (Tn) profile system was operated at  $z_1 = 0.04$  m,  $z_2 = 0.2$  m and  $z_3 = 0.8$  m  
134 for the direct determination of transport times (for details see Plake and Trebs, 2013). Vertical  
135 profiles of NO, NO<sub>2</sub>, O<sub>3</sub> and CO<sub>2</sub> were measured at  $z_1$ ,  $z_2$ ,  $z_3$  and additionally at  $z_4 = 4.0$  m  
136 by a system described in detail by Plake et al. (2014). Briefly, NO was measured by detection

137 of the chemiluminescence produced during the reaction of NO and O<sub>3</sub> (TEI 42iTL Thermo  
138 Scientific, Waltham, USA). NO<sub>2</sub> was photolytically converted to NO by exposure of the sam-  
139 ple air to a Blue Light Converter (BLC, Droplet Measurement Technologies, Boulder, USA).  
140 O<sub>3</sub> mixing ratios were measured with a UV-absorption analyzer (TEI-49i, Thermo Scientific,  
141 Waltham, USA). The efficiency of the photolytic conversion of NO<sub>2</sub> to NO was determined  
142 by a back titration procedure involving the reaction of O<sub>3</sub> with NO using a gas phase titration  
143 system (SYCOS K-GPT, Ansyco GmbH, Karlsruhe, Germany). Details on the sampling  
144 schedule and time resolution of the trace gas profiles system are described in Plake et al.  
145 (2014).

146 This study is based on simultaneous operation of both vertical profile systems at identical  
147 heights and, thus, ~~is focused~~ focuses on the period from 19 August to 26 September 2011  
148 ~~were when~~ both systems were operational. Vertical profiles of temperature (HMT337,  
149 Vaisala, Helsinki, Finland), wind speed and direction (WS425, Vaisala, Helsinki, Finland)  
150 were installed at 0.2 m, 0.8 m, 1.5 m, 2.5 m, 4.0 m. Soil temperature (107L, Campbell Scien-  
151 tific Inc., Logan, USA) was measured at -0.02 m. Global radiation ( $G$ ) and the NO<sub>2</sub> photolysis  
152 frequency ( $J_{NO_2}$ ) were measured at a height of 2.5 m with a net radiometer (CNR1,  
153 Kipp&Zonen, Delft, Netherlands), and a filter radiometer (Meteorology Consult GmbH,  
154 ~~Glashütten~~ Königstein, Germany), respectively. The data of temperature, wind and radiation  
155 were recorded by a data logger (CR3000, Campbell Scientific) every 10 seconds. A three di-  
156 mensional sonic anemometer (CSAT-3, Campbell Scientific) placed at  $z_{ref} = 3.0$  m measured  
157 3D wind and temperature at 20 Hz and the data were recorded by a CR3000 data logger. The  
158 friction velocity ( $u_*$ ) and stability functions ( $z/L$ ) were computed using the TK3 software  
159 (see Mauder and Foken, 2011). Eddy covariance fluxes of O<sub>3</sub> were simultaneously measured  
160 and are described in detail by Plake et al. (2014).

## 161 2.3 Theory

162 The data analysis was carried out for three individual layers ( $L_{1-3}$ ), which were named in  
163 ascending order starting at the soil surface. Hence,  $L_1$  was the lowermost canopy layer be-  
164 tween the corresponding measurement heights  $z_{1-2}$  ( $\Delta z(L_1) = 0.16$  m),  $L_2$  the upper canopy  
165 layer between  $z_{2-3}$  ( $\Delta z(L_2) = 0.6$  m), and  $L_3$  the layer above the canopy between  $z_3$  and  $z_{ref}$   
166 ( $\Delta z(L_3) = 2.2$  m). As shown in Plake et al. (2014) the vertical trace gas gradients between  
167  $z_{ref}$  and  $z_4$  were negligible, allowing the use of mixing ratios measured at  $z_4$  for  $L_3$ .

### 168 2.3.1 Chemical timescales

169 The overall chemical timescale  $\tau_{ch}$  (in s) of the NO-NO<sub>2</sub>-O<sub>3</sub> triad (Lenschow, 1982) was cal-  
170 culated for each layer ( $L_i$ ,  $i = 1, 2, 3$ ) as:

$$171 \tau_{ch}(L_i) =$$
$$172 \frac{2}{\sqrt{j_{NO_2}(L_i)^2 + j_{NO_2}(L_i) \cdot k_3(L_i) + k_3(L_i)^2 \cdot (N_{O_3}(L_i) + N_{NO}(L_i))^2 + 2j_{NO_2}(L_i) \cdot k_3(L_i) \cdot (N_{O_3}(L_i) + N_{NO}(L_i) + 2N_{NO_2}(L_i))}}}$$

173 (2)

174 where  $N_{O_3}$ ,  $N_{NO}$  and  $N_{NO_2}$  are the number densities (in molecules cm<sup>-3</sup>) of O<sub>3</sub>, NO and NO<sub>2</sub>  
175 for  $L_{1-3}$ , and  $k_3$  the reaction rate constant of R3 (in cm<sup>3</sup> molecule<sup>-1</sup> s<sup>-1</sup>) according to Atkinson  
176 et al. (2004). Geometric means of the number densities at  $z_{1-4}$  were used in Eq. 2 to account  
177 for non-linear profiles (e.g.,  $N_{NO}(L_1) = \sqrt{N_{NO}(z_1) \cdot N_{NO}(z_2)}$ ).

178 Equation 2 gives the chemical time scale of reactions R1 and R3 derived from the  
179 O<sub>3</sub> chemical-budget equation, i.e., considering only the reactions between O<sub>3</sub>, NO and NO<sub>2</sub>  
180 and not taking into account reactions of other compounds (e.g., peroxy radicals and VOCs). It  
181 is defined as the time at which the mixing ratio of one of the compounds significantly changes  
182 from its initial value when reacting with the other ones. It can also be seen as the time re-

183 quired for reaching a new photostationary state following a change in O<sub>3</sub>, NO or NO<sub>2</sub> mixing  
184 ratios, or the reaction rate constants  $j_{NO_2}$  and  $k_3$  (see Ganzeveld et al., 2012). The underlying  
185 assumptions are:

- 186 - only source and sink terms of the “triad” are considered, which means other reactions  
187 (e.g. RO<sub>2</sub>+NO) are not included.
- 188 - covariance terms and other budget terms i.e. horizontal and vertical advection, flux di-  
189 vergence and change in O<sub>3</sub> mixing ratio  $d[O_3]/dt$  are neglected.

### 190 **2.3.2 NO<sub>2</sub> photolysis within the canopy**

191 The data gaps in the measured time series of  $j_{NO_2}$  (in s<sup>-1</sup>) above the canopy were filled using  
192 the parameterization of  $j_{NO_2}$  as a function of  $G$  (in W m<sup>-2</sup>) by Trebs et al. (2009). This ap-  
193 proach was also used to parameterize in-canopy  $j_{NO_2}$  from a vertical in-canopy profile of  $G$ .  
194 The latter was calculated as function of the  $LAI$  profile using the method of Monsi and Saeki  
195 (1953):

$$196 \quad G(LAI) = G_0 \cdot \exp(-k_{ex} \cdot LAI) \quad (3)$$

197 where  $G_0$  (in W m<sup>-2</sup>) is the above-canopy  $G$  and  $k_{ex}$  is the dimensionless extinction coeffi-  
198 cient of the canopy. In this study, the extinction coefficient of barley ( $k_{ex} = 0.69$  by Monteith  
199 and Unsworth (1990)) was used. First  $G(LAI)$  was deduced and then converted into  $j_{NO_2}$ . Fi-  
200 nally, geometric means of  $j_{NO_2}$  were calculated for  $j_{NO_2}(L_{1-3})$ .

### 201 **2.3.3 Transport times**

202 For  $L_3$ , height integrated transport times  $\tau_{tr}(L_3)$  (in s) were derived by multiplying the aero-  
203 dynamic resistance ( $R_a(L_3)$ ) (e.g., Hicks et al., 1987; Erisman et al., 1994) with the layer  
204 thickness ( $\Delta z(L_3)$ ) (cf. Stella et al., 2013):

205  $\tau_{tr}(L_3) = R_a(L_3) \cdot \Delta Z(L_3)$  (4)

206  $R_a(L_3) = \frac{1}{\kappa \cdot u_*} \left[ \ln \left( \frac{z_{ref}-d}{z_3-d} \right) - \Psi_H \left( \frac{z_{ref}-d}{L} \right) + \Psi_H \left( \frac{z_3-d}{L} \right) \right]$  (5)

207 where  $\kappa$  was the von-Kàrmàn constant (= 0.4),  $d$  the displacement height ( $d = 0.75 \cdot h_c$ ),  $\Psi_H$   
 208 the stability correction function for heat (Foken, 2008) and  $L$  the Obukhov length.

209 In the canopy,  $\tau_{tr}(L_i, i = 1,2)$  were derived from the vertical Tn profiles (Lehmann et al.,  
 210 1999; Plake and Trebs, 2013):

211  $\tau_{tr}(L_i) = \ln \left[ \frac{C_{Tn_{z_l}(L_i)}}{C_{Tn_{z_u}(L_i)}} \right] / \lambda$  (6)

212 where  $C_{Tn_{z_l}}$  and  $C_{Tn_{z_u}}$  were the measured Tn concentrations (in Bq m<sup>-3</sup>) at the lower ( $z_l$ ) and  
 213 upper ( $z_u$ ) heights of  $L_i$ , and  $\lambda$  the radioactive decay rate  $\lambda = \ln 2 / T_{0.5} = 0.0125 \text{ s}^{-1}$  (Hänsel  
 214 and Neumann, 1995).

### 215 3 Results

#### 216 3.1 Meteorological conditions and mixing ratios

217 During the field experiment, low and high NO<sub>x</sub> periods occurred that were directly coupled to  
 218 the wind direction and could be attributed to two contrasting synoptic conditions character-  
 219 ized by different wind speeds (see Moravek et al., 2014b). Fig. 1a displays the dominance of  
 220 south westerly winds at the site during 45 % of the field experiment and their relation to rela-  
 221 tively low NO<sub>x</sub> levels (< 3 ppb). Contrastingly, winds from the north eastern sector were  
 222 characterized by high NO<sub>x</sub> levels often above 13 ppb (Fig. 1a). High NO<sub>x</sub> episodes (up to  
 223 40 ppb) were accompanied with low wind speed (< 3 m s<sup>-1</sup>) and low NO<sub>x</sub> (< 5 ppb) with wind  
 224 speeds greater above 3 m s<sup>-1</sup> as shown in Fig. 1b. O<sub>3</sub> levels exhibited the opposite dependency

225 | ~~on wind speed, while  $\Gamma$~~ the measured CO<sub>2</sub> levels generally showed a similar pattern for high  
226 | and low NO<sub>x</sub> levels, ~~while O<sub>3</sub> levels exhibited the opposite dependency on ws.~~

227 | For further data analysis, defined criteria allowed to account for these specific relationships.  
228 | In order to clearly separate entire days (24 h) of contrasting conditions from each other, the  
229 | criteria were defined as low NO<sub>x</sub> or high NO<sub>x</sub> periods when (i) the mean daytime wind speed  
230 | ~~ws~~ was  $> 3 \text{ m s}^{-1}$  and the wind direction mainly ranged between 180 and 270°, or (ii) the  
231 | mean daytime wind speed ~~ws~~ was  $< 3 \text{ m s}^{-1}$  and the wind direction was mainly outside 180 –  
232 | 270°, respectively. The wind direction definition was fulfilled during 96 % of the low NO<sub>x</sub>  
233 | periods and during 84 % of the high NO<sub>x</sub> periods. Following these criteria, we identified  
234 | eleven and nine days as low and high NO<sub>x</sub> periods, respectively, which were ~~separately~~ ana-  
235 | lyzed separately.

### 236 | 3.2 Vertical profiles of trace gases

237 | Since the wind field ~~is the driver~~ drives of vertical exchange of scalars such as trace gases  
238 | between vegetation and the atmosphere (Finnigan, 2000), it affects their vertical distribution.  
239 | Passive tracers such as Rn and CO<sub>2</sub> are used especially at nighttime as indicators for vertical  
240 | exchange processes within plant canopies (e.g., Trumbore et al., 1990; Nemitz et al., 2009).  
241 | Generally, nighttime ~~ws values~~ wind speeds during of the low and high NO<sub>x</sub> periods were ac-  
242 | cordingly higher and lower, respectively. This was reflected by the in-canopy concentrations  
243 | of both Rn and CO<sub>2</sub> (Fig. 2a–d). During nighttime when both gases are exclusively emitted by  
244 | soil, a rather weak enrichment within the canopy (Fig. 2a,c) reflected higher ~~ws~~ wind speeds  
245 | and, thus, enhanced exchange during the low NO<sub>x</sub> periods. In comparison, during the high  
246 | NO<sub>x</sub> periods a strong in-canopy CO<sub>2</sub> and Rn accumulation was observed (Fig. 2b,d). During  
247 | daytime, photosynthesis prohibits the use of CO<sub>2</sub> as passive tracer, whereas Rn profiles are

248 still useful as no biological processes such as stomatal uptake affect its concentration  
249 (Lehmann et al., 1999). The vertical exchange is generally enhanced during daytime causing  
250 dilution of the in-canopy Rn concentrations, which was especially pronounced ~~in-during~~ the  
251 low NO<sub>x</sub> periods (Fig. 2a) and was less evident during the high NO<sub>x</sub> periods (Fig. 2b); ~~due to~~  
252 ~~with~~ generally lower wind speeds ~~s-during the latter periods~~.

253 The vertical distribution of O<sub>3</sub> (Fig. 2e,f) reflected a typical pattern with lower mixing ratios  
254 closer to the ground and higher mixing ratios above. The diurnal O<sub>3</sub> maximum occurred dur-  
255 ing the afternoon around 16:00 CET (= UTC+1). Nevertheless, in the low NO<sub>x</sub> periods the  
256 diurnal O<sub>3</sub> maximum was much less pronounced compared to the high NO<sub>x</sub> periods with  
257 35 ppb and 50 ppb, respectively. Furthermore, characteristic vertical O<sub>3</sub> distributions were  
258 observed during the low and high NO<sub>x</sub> periods. Nighttime O<sub>3</sub> gradients were less pronounced  
259 during the low NO<sub>x</sub> than during the high NO<sub>x</sub> periods. Median in-canopy values of O<sub>3</sub> were  
260 10-20 ppb and ~~were~~ 20-25 ppb above ~~the-~~ canopy during the low NO<sub>x</sub> periods (Fig. 2e). Dur-  
261 ing the high NO<sub>x</sub> periods 1-6 ppb ~~of O<sub>3</sub>~~ were measured in the canopy and ~~10-25 ppb above-~~  
262 ~~the~~ canopy ~~10-25 ppb~~ (Fig. 2f).

263 During both the low and the high NO<sub>x</sub> periods, significantly enhanced NO mixing ratios pre-  
264 vailed during the morning hours from 06:00 to 14:00 CET (Fig. 2g,h) with median diurnal  
265 maxima of 0.6 ppb and 7.2 ppb, respectively, both occurring at 10:00 CET (not visible in Fig.  
266 2h due to scaling). The NO mixing ratios decreased afterwards to approach nighttime minima.  
267 These were characterized by small vertical NO gradients during both periods. During low  
268 NO<sub>x</sub> nights, NO appeared to be mainly present in the in-canopy air layer, with median mixing  
269 ratios at z<sub>1</sub> and z<sub>2</sub> of ≤ 0.1 ppb. The median values at z<sub>1</sub> and z<sub>2</sub> during the high NO<sub>x</sub> periods  
270 were ≤ 0.3 ppb, respectively.

271 NO<sub>2</sub> mixing ratios were generally found to increase with height (Fig. 2i,j), featuring signifi-  
272 cantly stronger vertical differences during the high NO<sub>x</sub> periods. Similar to NO, also NO<sub>2</sub>  
273 mixing ratios were enhanced throughout the profile during the morning hours of both, low  
274 and high NO<sub>x</sub> periods, with corresponding values of 1–2.5 ppb and 6–14 ppb, respectively. At  
275 nighttime, comparable NO<sub>2</sub> mixing ratios of around 1 ppb prevailed during both periods at  $z_1$ .  
276 NO<sub>2</sub> showed stronger gradients above the canopy during the high NO<sub>x</sub> periods. The diurnal  
277 NO<sub>2</sub> minima during low and high NO<sub>x</sub> periods were observed between 12-16 CET and  
278 14-16 CET, respectively.

### 279 3.3 Vertical profiles of chemical timescales

280 The obtained values for  $\tau_{ch}$  were generally higher during nighttime than during daytime (Fig.  
281 3a,d,g) and ~~decrease~~increased from  $L_3$  to  $L_1$ . The validity of our applied criteria for separa-  
282 tion between low and high NO<sub>x</sub> periods, is shown by the median values (brown and green  
283 lines) that nearly adjoined the interquartile range of the overall data set. Significantly higher  
284  $\tau_{ch}$  values prevailed during nighttime of the high NO<sub>x</sub> periods, ranging from 300 to 2500 s in  
285  $L_{1-3}$ . In contrast, low NO<sub>x</sub> periods were characterized by  $\tau_{ch}$  of 250–800 s in  $L_{1-3}$ . However,  
286 during daytime  $\tau_{ch}$  was within 100–200 s in  $L_{1-3}$  for both periods. During the low NO<sub>x</sub> peri-  
287 ods  $\tau_{ch}$  values were slightly higher compared to the high NO<sub>x</sub> periods.

### 288 3.4 Vertical profiles of transport times

289 The median  $\tau_{tr}(L_3)$  of all data Fig. 3b was one order of magnitude smaller during noon than  
290 at midnight with 30 and 200 s, respectively. As for  $\tau_{ch}$  (Sect. 3.3), also in the case of  $\tau_{tr}$  the  
291 medians of the low and high NO<sub>x</sub> periods adjoined the interquartile range of the overall data  
292 set. For example,  $\tau_{tr}(L_3)$  in the low NO<sub>x</sub> periods never exceeded  $\tau_{tr}(L_3)$  in the high NO<sub>x</sub>  
293 periods (cf. Fig. 3b). The difference of  $\tau_{tr}(L_3)$  between noon and midnight was largest in the

294 | high  $\text{NO}_x$  and smallest during the low  $\text{NO}_x$  periods with 470 s and 40 s, respectively. Com-  
295 | pared to  $L_{1-2}$  (Fig. 3e,h), the extreme values of the entire  $\tau_{tr}$  data set were found above the  
296 | canopy in  $L_3$ . The overall  $\tau_{tr}$  minimum occurred during daytime of the low  $\text{NO}_x$  periods, and  
297 | the maximum during nighttime of the high  $\text{NO}_x$  periods in  $L_3$  ~~$L_3$~~ .

298 | The diurnal course of  $\tau_{tr}(L_2)$  from the entire data set in Fig. 3e exhibited a similar pattern as  
299 |  $\tau_{tr}(L_3)$ , with higher  $\tau_{tr}(L_2)$  during nighttime than during daytime. Representative nighttime  
300 | and daytime values were 200 and 100 s, respectively, and a similar nighttime separation be-  
301 | tween the low and high  $\text{NO}_x$  periods as in Fig. 3b ~~was~~is observed.

302 | In contrast, both diurnal  $\tau_{tr}(L_1)$  medians representing all data and the high  $\text{NO}_x$  periods (Fig.  
303 | 3h) were slightly higher during daytime between 08:00 and 13:00 CET than at nighttime with  
304 | around 200 and 75–175 s, respectively. ~~In~~During the low  $\text{NO}_x$  periods, the median  $\tau_{tr}(L_1)$   
305 | was relatively constant throughout the day with about 200 s. The pattern of  $\tau_{tr}(L_1)$  was gen-  
306 | erally opposite to  $L_{2-3}$ , with faster  $\tau_{tr}(L_1)$  in the high  $\text{NO}_x$  periods than in the low  $\text{NO}_x$  peri-  
307 | ods.

### 308 | 3.5 Vertical profiles of Damköhler numbers

309 | The values for  $DA(L_3)$  presented in Fig. 3c were generally smaller during daytime than dur-  
310 | ing nighttime. They exhibited a diurnal minimum of 0.2 and a maximum of 1.3 at 08:00 and  
311 | 21:00 CET, respectively. ~~In~~During the low  $\text{NO}_x$  periods, the difference of the  $DA(L_3)$  median  
312 | ( $0.2 < DA(L_3) < 0.3$ ), to a  $DA$  of unity was highest, whereas in the high  $\text{NO}_x$  periods  $DA(L_3)$   
313 | remained at higher median values ( $0.3 < DA(L_3) < 3.9$ ).

314 | In contrast, the diurnal course of  $DA(L_2)$  in Fig. 3f exhibited its maximum of 1.25 at  
315 | 15:00 CET and featured nighttime minima of about 0.3. The difference in  $DA(L_2)$  between  
316 | the low and high  $\text{NO}_x$  periods was not as pronounced as for  $DA(L_3)$ . ~~This~~~~It~~ ~~became~~was most

317 obvious from 15:00 to 24:00 CET with lower  $DA(L_2)$  in the low  $\text{NO}_x$  periods. Hence, both  
318  $DA(L_{2,3})$  values throughout the day were within or above the critical range for  $DA$  ~~or above~~  
319 under all conditions.

320 Interestingly, the diurnal course of  $DA(L_1)$  (Fig. 3i) appeared-nearly mirrored that of-inverted  
321 ~~to~~  $DA(L_3)$ , with highest and lowest  $DA$  during daytime and nighttime, respectively. The diur-  
322 nal median of  $DA(L_1)$  partly exhibited values below 0.1 (transport dominates) during  
323 nighttime of the high  $\text{NO}_x$  periods, values above unity (chemistry dominates) from 12:00 to  
324 17:00 CET under all conditions, and between 0.1 and unity during nighttime in the overall  
325 data set and in the low  $\text{NO}_x$  periods.

## 326 4 Discussion

### 327 4.1 Transport times and resistances

#### 328 4.1.1 Thermal stratification

329 The diurnal courses of the temperature differences  $\Delta T(L_{1-3})$  in Fig. 4a–c describe the stabil-  
330 ity in each layer. They clearly indicated ~~d~~ contrasting stability conditions in  $L_1$  and  $L_{2-3}$ . During  
331 daytime, negative values of  $\Delta T(L_{2-3})$  reflected unstable conditions, while positive  $\Delta T(L_1)$   
332 reflected stable conditions. In contrast, at nighttime these conditions were reversed. Similar  
333 diurnal cycles of stratifications are observed for other canopies (cf. Jacobs et al., 1994; Kruijt  
334 et al., 2000; Nemitz et al., 2000), and are known to decouple the lower canopy from the air  
335 layers above (cf. Fig. 4d). Canopy coupling regimes are typically classified according to the  
336 detection of coherent structures in high frequency time series of scalars such as temperature  
337 (e.g. Foken et al., 2012; Dupont and Patton, 2012). In our data set  $\Delta T(L_1)$  ~~could-be~~ was used  
338 to explain why  $\tau_{tr}(L_1)$  was generally smaller, i.e. transport was faster, during nighttime than

339 during daytime (Fig. 3h). The soil released stored heat as thermal plumes during nighttime  
340 that drove an in-canopy nighttime convection, which reached up to the height of the tempera-  
341 ture inversion as ~~explained-found~~ by Dupont and Patton (2012) or Jacobs et al. (1994). ~~This~~  
342 ~~effect caused the lower  $\tau_{tr}(L_1)$  during nighttime.~~ The  $\tau_{tr}(L_1)$  maximum of 200 s from  
343 08:00 to 13:00 CET could accordingly ~~been~~ attributed to positive  $\Delta T(L_1)$  values at that time  
344 indicating a stable stratification. ~~In all layers~~ The thermal stratification was stronger during  
345 the high  $\text{NO}_x$  periods and weaker during the low  $\text{NO}_x$  periods in all layers (Fig. 4a–c). This  
346 was caused by higher wind speeds during the low  $\text{NO}_x$  periods causing increased turbulence  
347 and mixing that yielded smaller ~~that yielded better mixing and thus the~~ vertical temperature  
348 differences ~~were smaller~~.

#### 349 4.1.2 Aerodynamic resistances and transport times

350 Aerodynamic resistances above ( $R_a$ ) and within the canopy ( $R_{ac}$ ) ~~are~~ are considered as im-  
351 portant input ~~parameters-variables~~ for modeling studies on surface-atmosphere exchange flux-  
352 es. They ~~represent~~ can be derived from the transport times through a layer, normalized by the  
353 layer thickness ( $R_{a(c)} = \tau_{tr}/\Delta z$ ). In cases when the thicknesses of two layers under consider-  
354 ation differ, the effectiveness of transport can be represented by the corresponding aerody-  
355 namic resistances. On the other hand, transport times are required to evaluate the influence of  
356 chemical reactions on fluxes (e.g.,  $DA$ ).

357 ~~Aerodynamic in-canopy resistances~~ Typically, ( $R_{ac}$ ) values ~~are typically~~ parameterized as  
358 function of  $u^*$  and  $LAI$  (e.g., van Pul and Jacobs, 1994; Personne et al., 2009). These parame-  
359 terizations are based on experiments above e.g., crops such as maize (van Pul and Jacobs,  
360 1994) and consider a homogeneous vertically leaf distribution (Personne et al., 2009). How-  
361 ever, this approximation may differ substantially within grassland canopies, as their structure  
362 is characterized by high biomass density in the lowest layer (cf. Sect. 2.1).

363 The ~~usefulness-importance~~ of our results is underlined by the direct assessment of measured  
364  $R_{ac}$  values. From Eq. 6 we can assess  $R_{ac}$  for different canopy layers ( $L_1$ ,  $L_2$  and for the  
365 whole canopy ( $\tau_{tr}(z_1, z_3); \Delta z = z_3 - z_1$ ) ~~within-of~~ the grassland ~~canopy~~ (cf. Fig. 5). In the  
366 lower~~most~~ canopy ~~layer~~,  $R_{ac}(L_1)$  was generally highest with medians of 900 to 1000  $\text{s m}^{-1}$   
367 during nighttime and 1000 to 1300  $\text{s m}^{-1}$  during daytime (Fig. 5). In comparison, Gut et al.  
368 (2002) found the aerodynamic resistance in the lowest meter of an Amazonian rain forest  
369 canopy in a similar range ~~and showing the same diurnal pattern~~ with 600  $\text{s m}^{-1}$  during  
370 nighttime and 1700  $\text{s m}^{-1}$  during daytime, showing the same diurnal pattern.  
371 As found for the transport times, the diurnal course of  $R_{ac}$  ~~was inverted~~ in the upper layers  
372 ~~above-mirrored that of the lowermost layer~~ (Fig. 5). In the upper canopy, the median of  
373  $R_{ac}(L_2)$  typically ranged around 300  $\text{s m}^{-1}$  during nighttime and around 150  $\text{s m}^{-1}$  during day-  
374 time. In comparison, above the canopy the median of  $R_a(L_3)$  (Eq. 5) was substantially lower  
375 with around 80 and 15  $\text{s m}^{-1}$  during nighttime and daytime, respectively. Consequently, the  
376 aerodynamic resistances in and above the canopy ( $R_{ac}(L_{1,2})$  and  $R_a(L_3)$ ) differed by almost  
377 two orders of magnitude during daytime, and by one order of magnitude during nighttime.  
378 Accordingly, the efficiency of aerodynamic transport decreased with decreasing height, even  
379 if the transport times were partly-occasionally shorter in  $L_1$  compared to  $L_3$ . ~~The  $R_{ac}$  for the~~  
380 entire canopy (Fig. 5) reflects the sum of the measured transport times divided by the entire  
381 layer thickness ( $\Delta z = z_3 - z_1$ ) and can be considered as equivalent to a weighted average of  
382  $R_{ac}(L_1)$  and  $R_{ac}(L_2)$ . ~~for the whole canopy (Fig. 5)~~  $R_{ac}$  ranged in-between  $R_{ac}(L_1)$  and  
383  $R_{ac}(L_2)$  with 440  $\text{s m}^{-1}$  during nighttime and 360  $\text{s m}^{-1}$  during daytime. The opposite diurnal  
384 courses of both,  $R_{ac}(L_1)$  and  $R_{ac}(L_2)$  have an impact on  $R_{ac}$ , which in turn showed a smaller  
385 diurnal variation. As  $L_2$  contained around 80 % of the layer thickness between  $z_1$  and  $z_3$   
386 (cf. Fig. 5),  $R_{ac}$  was closer to  $R_{ac}(L_2)$ .

387 The median transport time through the 0.6 m high natural grassland canopy (also referred to  
388 as “canopy flushing time”) was presented in the related study of Plake and Trebs (2013) for  
389 the same experiment. It was measured using the vertical thoron profile between  $z_1$  and  $z_3$   
390 (Eq. 6). The canopy flushing time is consistent with the sum of  $\tau_{tr}(L_1)$  and  $\tau_{tr}(L_2)$  in this  
391 manuscript (cf. Fig. 7 below) and represents the in-canopy layer down to  $0.07 \cdot h_c$  ( $z_1/h_c$ ). It  
392 was determined to be  $\leq 6$  min exhibiting only small daytime/nighttime variation. Simon et al.  
393 (2005) reported canopy flushing times of around 60 min during any time of the day based on  
394 radon measurements within a 40 m high rain forest canopy. ~~For for~~ the layer between  $h_c$  and  
395  $0.13 \cdot h_c$  (canopy top to trunk space), ~~they determined flushing times of around 60 min during~~  
396 ~~any time of the day~~. As in the grassland canopy in Mainz-Finthen, nighttime in-canopy con-  
397 vection accounted for the small daytime/nighttime variation in their study. Normalization of  
398 their canopy flushing time by the layer thickness yielded  $R_{ac}$  in the order of  $100 \text{ s m}^{-1}$ , which  
399 is around 3–4 times lower than the corresponding  $R_{ac}$  of the grassland site. Other studies  
400 (Holzinger et al., 2005; Rummel, 2005) based on surface renewal models reported somewhat  
401 lower flushing times. Rummel (2005) found flushing times in a 32 m high rain forest canopy  
402 of  $\leq 200$  s during daytime, which correspond to  $R_{ac}$  values  $\leq 10 \text{ s m}^{-1}$ . In the same way  
403 Holzinger et al. (2005) determined flushing times of 90 s during daytime and around 300 s  
404 during nighttime within a 6 m high scrubby pine forest. Corresponding  $R_{ac}$  values were in the  
405 order of 20 and  $60 \text{ s m}^{-1}$ , respectively.

406 Thus, it is important to note that even if the canopy height of natural grassland canopies is  
407 small compared to forests (around 1–10 %); the corresponding canopy flushing times ~~are~~  
408 ofare within the same order of magnitude as those reported for forest canopies ~~(10–400 %)~~.  
409 The typically high biomass density in the lower canopy of grasslands (e.g., Jäggi et al., 2006;  
410 Nemitz et al., 2009) is the most obvious explanation. It provides a large aerodynamic re-

411 | sistance ( $> 900 \text{ s m}^{-1}$ ) in a small layer adjacent to the ground (here:  $R_{ac}(L_1)$ ). ~~The-This~~ aero-  
412 | dynamic resistance is large enough to increase the overall aerodynamic resistance of the  
413 | whole canopy ( $R_{ac}$ ) by 50 % and 140 % during night and daytime, respectively. Consequent-  
414 | ly,  $R_{ac}$  of the grassland canopy was found at least 3–4 times higher than  $R_{ac}$  values represent-  
415 | ing corresponding in-canopy layers of forests taken from literature.

416 | Plake and Trebs (2013) compared their directly measured transport times with the parameteri-  
417 | zations of van Pul and Jacobs (1994) and Personne et al. (2009). They found that none of the  
418 | parameterizations was able to reproduce the entire diurnal course of the in-canopy transport.  
419 | ~~An-a~~ Agreement with the measured transport times was either found during daytime (Personne  
420 | et al., 2009) or nighttime (van Pul and Jacobs, 1994), underlining the need for more direct  
421 | measurements on in-canopy transport.

## 422 | **4.2 Chemical timescales**

423 | The non-linear profiles of NO, NO<sub>2</sub> and O<sub>3</sub> might have introduced uncertainties in  $\tau_{ch}(L_{1-3})$ .  
424 | The potential uncertainties due to averaging were investigated by determining the individual  
425 |  $\tau_{ch}(z_{1-4})$  and their subsequent comparison with  $\tau_{ch}(L_{1-3})$ . In  $L_1$ ,  $L_2$  and  $L_3$  they were found  
426 | to be  $\leq 13 \%$ ,  $\leq 4 \%$  and  $\leq 2 \%$ , respectively, during daytime under any condition. During  
427 | nighttime, the uncertainties in  $L_2$  and  $L_3$  were found to be 6 and 2 % during the low NO<sub>x</sub> peri-  
428 | ods and 57 % and 13 % during the high NO<sub>x</sub> periods, respectively. In  $L_1$  the uncertainty dur-  
429 | ing nighttime was 30 % for all conditions. Furthermore, the in-canopy parameterization of  
430 |  $j_{NO_2}$  might have introduced additional uncertainties since (i) in reality the attenuation of in-  
431 | canopy radiation might be more complex than described in Eq. 3, and (ii) the parameterization  
432 | of  $j_{NO_2}$  from  $G$  is prone to uncertainties of  $>40 \%$  for  $G < 100 \text{ W m}^{-2}$ , 10 – 40 % for  $G = 100$ –  
433 |  $500 \text{ W m}^{-2}$  and  $\leq 10\%$  for  $G > 500 \text{ W m}^{-2}$  (Trebs et al., 2009). Moreover, omitting the influ-

434 ence of peroxy radical (HO<sub>2</sub>+RO<sub>2</sub>) levels for the calculation of the chemical timescales intro-  
435 duces uncertainties. However, measurements of vertical profiles of HO<sub>2</sub>+ RO<sub>2</sub> inside and  
436 above the grassland canopy are challenging and were not made during our experiment. Addi-  
437 tionally, no straightforward analytical framework exists to calculate their influence on chemi-  
438 cal timescales due to the variety of compounds and reaction rates involved in the complex  
439 HO<sub>2</sub>/RO<sub>2</sub> chemistry, which would require numeral modelling (see Heal et al., 2001).

440 The diurnal maxima and minima of  $\tau_{ch}(L_{1-3})$  (Fig. 3a,d,g) were found to coincide with the O<sub>3</sub>  
441 minima and maxima (Fig. 2e,f), respectively. The impact of the terms in Eq. 2 on  $\tau_{ch}(L_3)$  was  
442 examined by a correlation coefficient analysis. It was found to be highest for O<sub>3</sub> followed by  
443 NO<sub>2</sub> and NO with  $r = -0.57$ ,  $r = 0.46$  and  $r = -0.07$ , respectively. Consequently, the chemical  
444 timescale is dominated by the influence of O<sub>3</sub> as long as O<sub>3</sub> is present in excess compared to  
445 the other compounds. As the average air-chemical situation-conditions in Mainz-Finthen, was  
446 were characterized by a surplus of O<sub>3</sub> compared to NO<sub>2</sub> or NO (cf. Sect. 3.2), the magnitude  
447 of  $\tau_{ch}(L_3)$  was most affected by the mixing ratios of O<sub>3</sub>. In contrast, NO was generally less  
448 abundant, which explained the low overall impact on  $\tau_{ch}(L_3)$ . Only under-during high NO<sub>x</sub>  
449 situationsperiods, when NO levels were above 5 ppb (cf. Sect. 3.1), an increased impact of  
450 NO on  $\tau_{ch}(L_3)$  was found.

451 Fig. 6a summarizes the chemical timescales. The temporal variation in  $\tau_{ch}$ , expressed by  
452 higher nighttime and lower daytime values, can be considered as a rather typical pattern based  
453 on the diurnal courses of NO, NO<sub>2</sub> and O<sub>3</sub> (Fig. 2e-j) and their strong photochemical link.  
454 The vertical variation in  $\tau_{ch}(L_{1-3})$  was on the one hand caused by the attenuation of  $j_{NO_2}$  in  
455 the canopy, and on the other hand by generally increasing mixing ratios of NO, NO<sub>2</sub> and O<sub>3</sub>  
456 with height (Fig. 2e-j). It should be noted, that the latter finding was-is a siteexclusively valid  
457 characteristic issuefor this experimental site. Plake et al. (2014) measured insignificant soil

458 ~~biogenic~~ NO ~~soil~~ emissions ~~were measured by Plake et al. (2014), and were~~ underlined by  
459 weak in-canopy NO gradients (Fig. 2g,h). As already discussed in the previous paragraph,  
460 generally low NO, NO<sub>2</sub> and O<sub>3</sub> mixing ratios tend to cause high  $\tau_{ch}$ -values and vice versa.  
461 Consequently, at a site with higher NO emissions as e.g., an intensively managed agricultural  
462 field, the vertical  $\tau_{ch}$  profile would most likely feature smaller vertical differences.

463 The extremely high  $\tau_{ch}(L_1)$  during nighttime of the high NO<sub>x</sub> periods (Fig. 6a) were a direct  
464 consequence of canopy decoupling (cf. Sect. 4.1.1). Transport of O<sub>3</sub> and NO<sub>2</sub> into the lower  
465 canopy was suppressed by the temperature inversion (cf. Fig. 2f,j). The residual O<sub>3</sub> and NO<sub>2</sub>  
466 molecules were convectively circulated within the lower canopy and, subsequently deposited  
467 efficiently to surfaces until both almost disappeared in the early morning (Fig. 2f,j). ~~Thus~~Con-  
468 sequently, both the negligible NO emissions ~~together with~~ and the suppressed supply of O<sub>3</sub>  
469 and NO<sub>2</sub> from above, yielded ~~simultaneously~~ very low mixing ratios of all three ~~specie~~trace  
470 gases, that in turn led to the ~~extremely very~~ high  $\tau_{ch}(L_1)$  values.

471 Our results are in line with those of Stella et al. (2013) who reported median diurnal  $\tau_{ch}$  of  
472 80-300 s and 150-600 s above and within the canopy, respectively, for an intensively man-  
473 aged meadow. Their in-canopy  $\tau_{ch}$  maximum was somewhat lower than in Mainz-Finthen,  
474 which might be attributed to NO soil emissions or to averaging of different layers.

475 As mentioned above, the chemistry of HO<sub>2</sub>/RO<sub>2</sub> is not considered in our study. The reaction  
476 rate constant of NO + HO<sub>2</sub>/RO<sub>2</sub> is about 500 times higher than that of the reaction NO + O<sub>3</sub>.  
477 Assuming relatively high average daytime HO<sub>2</sub> + RO<sub>2</sub> mixing ratios of 60 ppt inside the can-  
478 opy (see Wolfe et al., 2014) the oxidation of NO to NO<sub>2</sub> would be as fast as with 30 ppb of  
479 O<sub>3</sub>. This implies that these chemical timescales may be comparable to those of the reaction  
480 NO + O<sub>3</sub>, which dominates  $\tau_{ch}$  derived from Eq. 2. However, it should be noted that perox-  
481 ides have a high affinity to be lost at surfaces, which may reduce their presence in dense

482 ~~grassland canopies. Since Eq. 2 exclusively considers R1 and R3, additional reactions may~~  
483 ~~have biased the obtained  $\tau_{ch}$  values to a certain extent. For instance, the oxidation of NO to~~  
484 ~~NO<sub>2</sub> by peroxy radicals (Sect. 1); Additionally, -or~~ reactions between volatile organic com-  
485 pounds (VOCs) and O<sub>3</sub> (e.g., Atkinson and Arey, 2003) might have influenced ~~ambient NO,~~  
486 ~~NO<sub>2</sub> and O<sub>3</sub> levels~~ chemical timescales. Simultaneously measured biogenic VOC mixing rati-  
487 os featured very small values at our site (e.g., isoprene < 0.7 ppb, monoterpene < 0.3 ppb,  
488 J. Kesselmeier, personal communication). Due to the absence of measurements the influence  
489 of anthropogenic VOCs is not taken into account. ~~Thus, the latter reactions could be consid-~~  
490 ~~ered of minor importance, whereas information on peroxy radicals was unfortunately not~~  
491 ~~available.~~

### 492 **4.3 Influence of meteorology and air pollution on vertical Damköhler number profiles**

493 The summarized daytime  $DA(L_{1-3})$  in Fig. 6c exhibited ~~a pattern of~~ decreasing  $DA$  values  
494 with increasing layer height. Thus, the likelihood of chemical flux divergence ~~was indicated~~  
495 ~~to~~ decreased from  $L_1$  to  $L_3$ . Throughout  $L_1$  to  $L_3$ , the  $\tau_{ch}$  values (Fig. 6a) showed a lower var-  
496 iation compared to the corresponding  $\tau_{tr}$  values (Fig. 6b). ~~Therefore~~ Hence, the daytime  $DA$   
497 profile was mainly caused by the vertical  $\tau_{tr}$  profile.

498 Interestingly, the nighttime  $DA$  ~~of for all data~~ and the high NO<sub>x</sub> periods ~~data~~ showed opposite  
499 vertical profiles, indicating an increasing likelihood of chemical flux divergence with increas-  
500 ing layer height ( $L_1$  to  $L_3$ ). This was especially pronounced during nighttime of the high NO<sub>x</sub>  
501 periods, where the only instance without indication for a flux divergence within the entire  
502 data set for  $L_1$  was found ~~for  $L_1$~~ . The reasons for this were (i) the extraordinary-very high  
503  $\tau_{ch}(L_1)$  (Fig. 6a and Sect. 4.2), and (ii) the reversed vertical transport time profiles during  
504 nighttime (fastest in  $L_1$ ) of the high NO<sub>x</sub> periods (Fig. 6b). This finding agrees very well with

505 Rummel (2005) who found ~~at nighttime that~~ the transport timescale in the ~~lowest-lowermost~~  
506 layer of an Amazonian rainforest ~~to be~~ faster than the chemical timescale ~~of the NO-NO<sub>2</sub>-O<sub>3</sub>~~  
507 ~~triad during nighttime.~~

508 Above the canopy, the order of magnitude (Fig. 6c) and the median diurnal course (Fig. 3c) of  
509 *DA* compared well with the values of Stella et al. (2013). ~~But~~ ~~†~~ The in-canopy *DA* of Stella et  
510 al. (2013) was smaller than the *DA* above the canopy throughout the entire day, which is in  
511 contrast to our study. Considering the average canopy flushing time given in Plake and Trebs  
512 (2013) (cf. Sect. 4.1.2) and the  $\tau_{ch}(L_2)$  (cf. Fig. 6a), ~~a comparable the average~~ in-canopy *DA*  
513 in Mainz-Finthen was in the order of 2 and 1 for daytime and nighttime, respectively. Thus, in  
514 our study in-canopy *DA* ~~in our study values~~ are on average significantly higher than above the  
515 canopy throughout the day. ~~As the canopy height in Stella et al. (2013) was only around~~  
516 ~~0.2 m, the corresponding transport time was faster with 80 s at noon which could explain the~~  
517 ~~lower in canopy DA compared to our study.~~ Finally, it should be noted that in-canopy, *DA*  
518 values ~~within plant canopies may not be fully representative as are not fully representative for~~  
519 ~~all processes, since~~ besides transport and chemistry, additional sources and sinks for trace  
520 gases exist within plant canopies. These are specific for each trace gas and will be further dis-  
521 cussed below.

## 522 4.4 Implications for measured fluxes

### 523 4.4.1 Potential NO<sub>x</sub> canopy reduction

524 Within the canopy,  $DA(L_{1-2})$  (Fig. 3f,i; Fig. 6c) suggested that chemical reactions exhibited a  
525 larger influence on the NO-NO<sub>2</sub>-O<sub>3</sub> triad during daytime than during night. However, reactive  
526 trace gases in canopies are deposited to soil and vegetation elements. Trace gases can be ef-  
527 ficiently taken up by plants due to adsorption/absorption on cuticles and diffusion through

528 stomata (e.g., Breuninger et al., 2012). On the other hand, particularly NO is simultaneously  
 529 produced by microbial processes and is subsequently released from soil. Although, the latter  
 530 process could be neglected in this study due to insignificant NO soil emissions (Sect. 4.2), the  
 531 uptake of NO<sub>2</sub> by plants, however, was investigated in order to draw ~~general~~ conclusions on  
 532 potential NO<sub>x</sub> canopy reduction within natural grasslands canopies. Hence, ~~additional infor-~~  
 533 ~~mation on~~ the characteristic time scale of plant uptake ( $\tau_u$ ) of NO<sub>2</sub> ~~was required. Such time-~~  
 534 ~~scales  $\tau_u(NO_2)$~~  integrated over the whole canopy ( $L_{1+2}$ ) ~~were~~ was estimated based on a re-  
 535 sistance model (Baldocchi, 1988), following an approach of Rummel (2005) as:

$$536 \quad \tau_u(x) = \left( \frac{1}{R_{Lx}} \cdot \frac{\Delta LAI}{\Delta z} \right)^{-1} \quad (7)$$

537 where  $x$  denoted the trace gas of interest (here  $x = \text{NO}_2$ ) and  $R_{Lx}$  was the leaf resistance of  $x$ :

$$538 \quad R_{Lx} = \left( \frac{1}{R_{blx} + R_{sx} + R_{mesx}} + \frac{2}{R_{blx} + R_{cutx}} \right)^{-1} \quad (8)$$

539 with  $R_{blx}$  being the leaf boundary layer resistance of  $x$  calculated according to Personne et al.  
 540 (2009),  $R_{sx}$  the stomatal resistance of  $x$  taken from Plake et al. (2014),  $R_{mesx}$  the mesophyll  
 541 resistance set to 200 s m<sup>-1</sup> for NO<sub>2</sub> and  $R_{cutx}$  the cuticular resistance set to 9999 s m<sup>-1</sup> due to  
 542 the unimportance of cuticular deposition for NO<sub>2</sub> (both values were taken from Stella et al.  
 543 (2013)).

544 During daytime, the median of  $\tau_u(NO_2)$  calculated from all data was typically found to be the  
 545 shortest amongst all timescales relevant for NO<sub>2</sub>, typically ranging between 90 and 160 s  
 546 between 09:00 and 17:00 CET (Fig. 7). This timescale was closely followed by  $\tau_{ch}(L_{1+2})$   
 547 exhibiting values between 100 and 200 s in the same time window period, but ~~with a shorter~~  
 548 lasting the minimum was slightly skewed towards the afternoon. In contrast, the ~~values of~~  
 549  $\tau_{tr}(L_{1+2})$  the canopy flushing time,  $\tau_{tr}(L_{1+2})$  ranged from 250 to 290 s (Fig. 7) during this

550 | time. For a ~~similar-comparable natural grassland~~ canopy with significant NO soil emissions,  
551 | this would imply an efficient in-canopy conversion of NO to NO<sub>2</sub> during daytime, followed  
552 | by an effective NO<sub>2</sub> plant uptake as the transport was found to be 2-3 times slower. Further-  
553 | more, the biomass density within the lowest 0.2 m of the canopy (i) strongly inhibits the  
554 | transport, especially in  $L_1$  during daytime (Fig. 5; Fig. 6b), and (ii) ~~dampens-attenuates~~ the  
555 | photolysis of NO<sub>2</sub> at the soil-canopy interface, the location where NO is usually emitted. This  
556 | indicates that a strong potential for NO<sub>x</sub> canopy reduction ~~occurring-exists~~ in such grassland  
557 | ecosystems during daytime, if-in case the precondition of significant NO soil emissions is  
558 | fulfilled. The presence of peroxy radicals may even amplify this process.  
559 | However, during nighttime,  $\tau_u(NO_2)$  was found to be very large (Fig. 7) due to plant stomata  
560 | closure. Hence, the role of turbulence-chemistry interactions ( $DA(L_{1-2})$ ) was dominating  
561 | over biological uptake processes. In  $L_1$  the transport of soil emitted NO would be slowest un-  
562 | der relatively windy nighttime situations (low NO<sub>x</sub> periods in Fig. 3h) due to undeveloped in-  
563 | canopy convection. Thus, a considerably high mixing ratio of O<sub>3</sub> within the canopy (Fig. 2e)  
564 | would lead to an efficient formation of NO<sub>2</sub> indicated by  $DA(L_{1-2})$  close to unity. The uptake  
565 | of NO<sub>2</sub> by plants would be insignificant (see above), and only soil deposition would lead to a  
566 | small NO<sub>2</sub> depletion. Most likely, such nighttime conditions would lead to simultaneous NO<sub>2</sub>  
567 | and NO canopy emission fluxes. During nights with low-~~ws-~~ wind speeds (high NO<sub>x</sub> periods),  
568 | the temperature inversion constitutes a “canopy lid”. Within the canopy ( $L_{1+2}$ ) the reaction of  
569 | residual O<sub>3</sub> (cf. Sect. 4.2) and soil emitted NO would compete with the O<sub>3</sub> deposition to sur-  
570 | faces-deposition. Subsequently, a mixture of NO and NO<sub>2</sub> would be trapped inside the cano-  
571 | py. Besides some minor in-canopy NO<sub>2</sub> losses (see above), a distinct NO and NO<sub>2</sub> release  
572 | may occur in the morning hours, which has been observed for forests (cf. Foken et al., 2012;  
573 | Dorsey et al., 2004; Jacob and Wofsy, 1990).

#### 574 4.4.2 Influence on O<sub>3</sub> deposition flux

575 Similar to NO<sub>2</sub>, the application of in-canopy DA values for O<sub>3</sub> remains difficult, since plant  
576 uptake and deposition to plant surfaces and the soil are additional O<sub>3</sub> ~~loss pathways besides~~  
577 ~~chemistry~~. The characteristic timescale of O<sub>3</sub> plant uptake and soil deposition  $\tau_u(O_3)$ , shown  
578 in Fig. 7, was estimated using Eqs. 7 and 8, with  $x = O_3$ ,  $R_{mes_x}$  set to 0 s m<sup>-1</sup> (Erisman et al.,  
579 1994) and  $R_{cut_x} = R_{ns_x} - R_{soil_x}$  (e.g., Lamaud et al., 2009).  $R_{ns_x}$  was taken from Plake et al.  
580 (2014) and  $R_{soil_x} = 240$  s m<sup>-1</sup> according to Lamaud et al. (2009).  $\tau_u(O_3)$  ranged from 30 to  
581 150 s, which clearly illustrates the dominance of in-canopy O<sub>3</sub> plant uptake and soil deposi-  
582 tion.  $\tau_u(O_3)$  was significantly faster than both  $\tau_{tr}(L_{1-2})$  and  $\tau_{ch}(L_{1-2})$  during the entire day  
583 (values are given in Sect. 4.4.1).

584 Consequently, only DA values above the canopy, i.e.  $DA(L_3)$  ~~in this study, are valid as an pro-~~  
585 ~~vides an indicator indication~~ for potential O<sub>3</sub> flux divergence. ~~Because Since~~ the  $DA(L_3)$  al-  
586 ways exceeded 0.1 (Fig. 3c, Fig. 6c), a chemical flux divergence could not be excluded at the  
587 Mainz-Finthen site. Furthermore,  $DA > 1$  (Fig. 3c) during the early evening hours clearly  
588 indicated ~~potential flux divergence~~ the dominance of chemical reactions over transport.  
589 ~~During~~ the low NO<sub>x</sub> periods, the probability ~~for~~ flux divergence was lowest. The influ-  
590 ence of chemistry on O<sub>3</sub> deposition fluxes determined by Plake et al. (2014) at the Mainz-  
591 Finthen grassland site will be discussed below. The median O<sub>3</sub> fluxes for the entire measure-  
592 ment period ranged from about -1.5 to -6 nmol m<sup>2</sup> s<sup>-1</sup> during night and daytime, respectively.

593 Due to negligible NO soil emissions, a chemical flux divergence in  $L_3$  resulting from counter-  
594 directed fluxes of NO and O<sub>3</sub> was very unlikely. Nevertheless, we used a simplified method  
595 proposed by Duyzer et al. (1995) based on R1 and R3 and the law of mass conservation to  
596 approximate. ~~T~~ the flux divergence ~~is approximated~~ by the correction factor  $\alpha_{O_3}$  as:

$$597 \quad \alpha_{O_3} = \frac{\phi_x}{\kappa \cdot u_*} \cdot [k_1 \cdot (N_{NO} \cdot F_{O_3}^* + N_{O_3} \cdot F_{NO}^*) - j_{NO_2} \cdot F_{NO_2}^*] \quad (9)$$

598 where  $\phi_x = \phi_{O_3} = \phi_H$  was the stability correction function for heat (Högström, 1988),  $F_{O_3}^*$   
 599 the measured  $O_3$  flux at  $z_{ref}$  determined by the eddy covariance method (cf. Plake et al.,  
 600 2014) and  $F_{NO}^*$  and  $F_{NO_2}^*$  the corresponding NO and  $NO_2$  fluxes determined by the dynamic  
 601 chamber technique (cf. Plake et al., 2014). The estimated  $O_3$  deposition flux at  $z_3$  ( $F_{z_3}$ ) was  
 602 then calculated as:

$$603 \quad F_{z_3} = F_{z_{ref}} + \int_{z_3}^{z_{ref}} \left( \frac{\partial F}{\partial z} \right)_z dz = F_{O_3}^* + \alpha_{O_3} \cdot z_3 \cdot \left( 1 + \ln \frac{z_{ref}}{z_3} \right) \quad (10)$$

604 where the term  $\int_{z_3}^{z_{ref}} \left( \frac{\partial F}{\partial z} \right)_z dz$  was the integrated flux divergence within  $L_3$ . The resulting  
 605 median  $O_3$  flux divergence was quantified to be less than 1 %, confirming ~~the our~~ a priori  
 606 ~~assumption of irrelevant  $O_3$  flux divergence.~~

607 Nevertheless, we examined the influence of the enhanced NO mixing ratios in the morning  
 608 hours (Sect. 3.2, Fig. 2g,h), accompanied by very low  $O_3/NO$  ratios (Fig. 8) on the measured  
 609  $O_3$  fluxes. A chemically induced  $O_3$  flux  $F_c(O_3)$  due to production  $P(O_3)$  or loss  $L(O_3)$  of  $O_3$   
 610 by R1 and R3 integrated over the air column of  $L_3$  was quantified according to Rummel et al.  
 611 (2007) as:

$$612 \quad F_c(O_3) = P(O_3) - L(O_3) = \int_{z_3}^{z_{ref}} \frac{\mu_{NO_2}(z) \cdot \rho_d(z)}{\tau_{NO_2}(z)} \cdot dz - \int_{z_3}^{z_{ref}} \frac{\mu_{O_3}(z) \cdot \rho_d(z)}{\tau_{O_3}(z)} \cdot dz \quad (11)$$

613 where  $\rho_d$  (in  $\text{mol m}^{-3}$ ) was the molar density of dry air.  $\tau_{NO_2}$  and  $\tau_{O_3}$  (in s) were the chemical  
 614 depletion times of  $NO_2$  and  $O_3$ , respectively:

$$615 \quad \tau_{NO_2} = \frac{1}{j_{NO_2}} \quad (12)$$

$$616 \quad \tau_{O_3} = \frac{1}{k_1 \cdot N_{NO}} \quad (13)$$

617 Fig. 9a displays the diurnal courses of  $P(O_3)$  and  $L(O_3)$  exhibiting median values of  
618 0 to 1.9  $\text{nmol m}^{-2} \text{s}^{-1}$  and 0 to -1.4  $\text{nmol m}^{-2} \text{s}^{-1}$ , respectively. The ~~maximum-maximal~~ median  
619 values were related to the enhanced  $\text{NO}_x$  levels in the morning. The resulting median net  
620  $F_c(O_3)$  in Fig. 9b ranged between 0.6 and -0.05  $\text{nmol m}^{-2} \text{s}^{-1}$ , representing a net  $\text{O}_3$  production  
621 in  $L_3$  during daytime and a net loss during nighttime. Repeatedly, the medians of low and  
622 high  $\text{NO}_x$  periods adjoined the interquartile range of the overall data set, showing a variability  
623 of one order of magnitude of net  $F_c(O_3)$  during daytime. Considering the median values of all  
624 data, the ~~measured-chemical contribution to the measured EC flux of  $\text{O}_3$  deposition-flux~~  
625 would ~~be change by~~ around +10 % during daytime and -3 % during nighttime. Consequently,  
626 the actual daytime  $\text{O}_3$  deposition to the canopy is higher than measured by the EC method.  
627 This finding is interesting, as to our knowledge previous studies only reported chemical  $\text{O}_3$   
628 losses ~~above the canopy when dealing with the chemical flux divergence of  $\text{O}_3$ . The due to~~  
629 outbalancing of the reactions of  $\text{O}_3$  with  $\text{NO}$  (e.g., Dorsey et al., 2004) or VOCs (e.g., Kurpius  
630 and Goldstein, 2003) emitted by soil or plants, respectively, ~~resulted in net  $\text{O}_3$  loss~~. The net  
631  $\text{O}_3$  production in our study was attributed to a deviation from the  $\text{NO-NO}_2\text{-O}_3$  photostationary  
632 state by a surplus of  $\text{NO}_2$ , based on  $\text{NO}$  oxidation by e.g. peroxy radicals or other oxidants (cf.  
633 Trebs et al., 2012). Unfortunately, we were not able to assess the impact of these reactions  
634 involved in the net  $\text{O}_3$  production on the calculated chemical timescales as measurements of  
635 peroxy radicals were not available. The  $\text{NO}_2$  surplus might have originated from simultaneous  
636 emissions of non-methane hydrocarbons, carbon monoxide ( $\text{CO}$ ) and  $\text{NO}$  from motorways  
637 surrounding the site in a distance of some kilometers. It is well known that under daytime  
638 conditions peroxy radicals are formed that can oxidize  $\text{NO}$  without consumption of  $\text{O}_3$  result-  
639 ing in net  $\text{O}_3$  production (Seinfeld and Pandis, 2006). Although, this  $\text{O}_3$  production might also  
640 prevail at other experimental sites, this effect is most likely balanced or even exceeded by the

641 destruction of O<sub>3</sub> due to biogenic soil NO emissions which were negligible at our site (a nutri-  
642 ent poor grassland site).

## 643 5 Conclusions

644 For the first time, we simultaneously measured transport times (aerodynamic resistances),  
645 vertical profiles of NO-NO<sub>2</sub>-O<sub>3</sub> mixing ratios and micrometeorological quantities within and  
646 above a natural grassland canopy. The obtained data were analyzed to gain insights about the  
647 potential NO<sub>x</sub> canopy reduction in the grassland canopy, and to analyze the effect-contribution  
648 of chemistry on fluxes of purely depositing compounds, such as O<sub>3</sub>. We observed two ex-  
649 tremes regimes: a) ~~the first characterized by~~ high wind speed and low NO<sub>x</sub> mixing ratios (low  
650 NO<sub>x</sub> periods) and b) ~~the second by~~ low wind speed and high NO<sub>x</sub> mixing ratios (high NO<sub>x</sub>  
651 periods). Our study highlights that ~~(i)~~ as a result of in-canopy convection, nighttime transport  
652 in the lowest-lowermost canopy layer is fastest, while during highly stable conditions above  
653 the canopy are highly stable related due to low wind speed ~~(during the high NO<sub>x</sub> periods)~~.

654 Interestingly, our results on transport-chemistry interactions within the grassland canopy are  
655 partly comparable to those found in the Amazonian rainforest, although the vertical canopy  
656 structure differs substantially. Natural grasslands exhibit very high biomass densities in the  
657 lowest canopy part. Thus, the median aerodynamic resistance in the lowest canopy layer  
658 (0.04–0.2 m) was found to be of the same magnitude (> 900 s m<sup>-1</sup>) and to feature the same  
659 diurnal pattern (higher during daytime, lower at night) as the aerodynamic resistance in-de-  
660 termined for the lowest meter of an Amazonian rain forest. The median in-canopy aerody-  
661 namic resistance representing the whole grassland canopy was at least 3–4 times higher than  
662 in-canopy aerodynamic resistances of forest canopies available from literature. Our results  
663 reveal that even if the canopy height of natural grassland canopies is small compared to for-

664 | ests (around 1–10 %), the corresponding canopy flushing times are ~~of the same~~ of the same  
665 | order of magnitude as those reported for forest canopies ~~(10–400 %)~~. The median canopy  
666 | flushing times exhibited only small daytime/nighttime variability, which is ~~well~~ in accordance  
667 | with a detailed study on flushing times within an Amazonian rain forest (Simon et al., 2005).  
668 | The small daytime/nighttime variability is caused by the compensating transport efficiencies  
669 | in the lower and upper canopy layers during daytime and nighttime for both canopy types.

670 | The median canopy flushing time of the grassland was found to be  $\leq 6$  min and the chemical  
671 | timescale of the NO-NO<sub>2</sub>-O<sub>3</sub> triad during daytime ranged between 1–3 min. This has obvious  
672 | implications e.g., for soil emitted reactive compounds such as NO, potentially implying fast  
673 | chemical conversion of NO to NO<sub>2</sub> within the grassland canopy. During daytime the plant  
674 | uptake of NO<sub>2</sub> was shown to be 2–3 times faster than the canopy flushing time. Inevitably,  
675 | this leads to a strong potential NO<sub>x</sub> canopy reduction in the presence of biogenic NO soil  
676 | emissions. This effect may be amplified in case substantial levels of peroxy radicals prevail  
677 | inside the canopy. Due to the extensive global terrestrial coverage with grassland canopies,  
678 | this finding is highly relevant for the application of global chemistry and transport models.

679 | Our results ~~clearly reveal~~indicate that the daytime NO<sub>x</sub> canopy reduction for grasslands ~~to~~  
680 | may be be much higher than 64 %. Nevertheless, an improved daily averaged for the NO<sub>x</sub>  
681 | canopy reduction factor in analogy to ~~the one in~~ Yienger and Levy (1995) cannot be presented  
682 | here due to the insignificant NO soil emissions at the experimental al site.

683 | Moreover, W~~we~~ determined a median net chemical O<sub>3</sub> production of 10 % during daytime  
684 | within the air column between the EC flux measurement and the canopy, which was due to  
685 | the absence of soil biogenic NO ~~soil~~ emission in our study. Hence, in contrast to previous  
686 | studies our measured O<sub>3</sub> deposition flux by ~~eddy covariance~~EC is slightly underestimated.  
687 | The chemical flux divergence for O<sub>3</sub> was one order of magnitude larger during the high NO<sub>x</sub>

688 than during the low NO<sub>x</sub> periods. In-canopy Damköhler numbers were shown to be relevant  
689 for NO<sub>2</sub> only under nighttime conditions, which was due to the minor role of NO<sub>2</sub> uptake by  
690 plants at this time. ~~Above the canopy~~ Damköhler numbers above the canopy indicated a po-  
691 tential flux divergence, but did not provide a hint for the observed chemical production of O<sub>3</sub>.  
692 The only instance without indication for a chemical flux divergence within the entire data set  
693 was found during nighttime of the high NO<sub>x</sub> periods in the ~~lowest~~lowermost canopy layer.

## 694 **Acknowledgements**

695 This project was funded by the Max Planck Society. We are grateful to J.-C. Mayer for the  
696 installation and the maintenance of meteorological sensors and for supporting the data evalua-  
697 tion. We are indebted to A. Moravek for his support with the eddy covariance measurements  
698 and the corresponding data evaluation and the fruitful discussions on many details of this  
699 study.

700

## 701 **References**

- 702 Atkinson, R., and Arey, J.: Gas-phase tropospheric chemistry of biogenic volatile organic  
703 compounds: a review, *Atmospheric Environment*, 37, S197-S219, DOI 10.1016/S1352-  
704 2310(03)00391-1, 2003.
- 705 Atkinson, R., Baulch, D. L., Cox, R. A., Crowley, J. N., Hampson, R. F., Hynes, R. G.,  
706 Jenkin, M. E., Rossi, M. J., and Troe, J.: Evaluated kinetic and photochemical data for  
707 atmospheric chemistry: Volume I - gas phase reactions of O<sub>(x)</sub>, HO<sub>(x)</sub>, NO<sub>(x)</sub> and SO<sub>(x)</sub> species,  
708 *Atmos Chem Phys*, 4, 1461-1738, 2004.
- 709 Aylor, D. E., Wang, Y. S., and Miller, D. R.: Intermittent wind close to the ground within a  
710 grass canopy, *Boundary-Layer Meteorology*, 66, 427-448, 1993.
- 711 Bakwin, P. S., Wofsy, S. C., Fan, S. M., Keller, M., Trumbore, S. E., and Dacosta, J. M.:  
712 Emission of nitric-oxide (NO) from tropical forest soils and exchange of NO between the  
713 forest canopy and atmospheric boundary-layers, *Journal of Geophysical Research-*  
714 *Atmospheres*, 95, 16755-16764, 1990.
- 715 Baldocchi, D.: A multi-layer model for estimating sulfur-dioxide deposition to a deciduous  
716 oak forest canopy, *Atmospheric Environment*, 22, 869-884, DOI 10.1016/0004-  
717 6981(88)90264-8, 1988.

- 718 Breuninger, C., Oswald, R., Kesselmeier, J., and Meixner, F. X.: The dynamic chamber  
719 method: trace gas exchange fluxes (NO, NO<sub>2</sub>, O<sub>3</sub>) between plants and the atmosphere in the  
720 laboratory and in the field, *Atmos Meas Tech*, 5, 955-989, DOI 10.5194/amt-5-955-2012,  
721 2012.
- 722 Crutzen, P.: Discussion of chemistry of some minor constituents in stratosphere and  
723 troposphere, *Pure Appl Geophys*, 106, 1385-1399, DOI 10.1007/Bf00881092, 1973.
- 724 Denmead, O. T., Freney, J. R., and Dunin, F. X.: Gas exchange between plant canopies and  
725 the atmosphere: Case-studies for ammonia, *Atmospheric Environment*, 42, 3394-3406, DOI  
726 10.1016/j.atmosenv.2007.01.038, 2007.
- 727 Dorsey, J. R., Duyzer, J. H., Gallagher, M. W., Coe, H., Pilegaard, K., Weststrate, J. H.,  
728 Jensen, N. O., and Walton, S.: Oxidized nitrogen and ozone interaction with forests. I:  
729 Experimental observations and analysis of exchange with Douglas fir, *Q J Roy Meteor Soc*,  
730 130, 1941-1955, DOI 10.1256/Qj.03.124, 2004.
- 731 Dupont, S., and Patton, E. G.: Momentum and scalar transport within a vegetation canopy  
732 following atmospheric stability and seasonal canopy changes: the CHATS experiment, *Atmos  
733 Chem Phys*, 12, 5913-5935, DOI 10.5194/acp-12-5913-2012, 2012.
- 734 Duyzer, J. H., Deinum, G., and Baak, J.: The interpretation of measurements of surface  
735 exchange of nitrogen-oxides - correction for chemical-reactions, *Philos T R Soc A*, 351, 231-  
736 248, DOI 10.1098/rsta.1995.0031, 1995.
- 737 Erisman, J. W., Vanpul, A., and Wyers, P.: Parametrization of surface-resistance for the  
738 quantification of atmospheric deposition of acidifying pollutants and ozone, *Atmospheric  
739 Environment*, 28, 2595-2607, DOI 10.1016/1352-2310(94)90433-2, 1994.
- 740 Finnigan, J.: Turbulence in plant canopies, *Annu Rev Fluid Mech*, 32, 519-571, DOI  
741 10.1146/annurev.fluid.32.1.519, 2000.
- 742 Foken, T.: *Micrometeorology*, Springer, Berlin, Heidelberg 306 pp., 2008.
- 743 Foken, T., Meixner, F. X., Falge, E., Zetzsch, C., Serafimovich, A., Bargsten, A., Behrendt,  
744 T., Biermann, T., Breuninger, C., Dix, S., Gerken, T., Hunner, M., Lehmann-Pape, L., Hens,  
745 K., Jocher, G., Kesselmeier, J., Luers, J., Mayer, J. C., Moravek, A., Plake, D., Riederer, M.,  
746 Rutz, F., Scheibe, M., Siebicke, L., Sörgel, M., Staudt, K., Trebs, I., Tsokankunku, A.,  
747 Welling, M., Wolff, V., and Zhu, Z.: Coupling processes and exchange of energy and reactive  
748 and non-reactive trace gases at a forest site - results of the EGER experiment, *Atmos Chem  
749 Phys*, 12, 1923-1950, DOI 10.5194/acp-12-1923-2012, 2012.
- 750 [Ganzeveld, L., Ammann, C., Loubet, B.: Review on modelling atmosphere biosphere ex-  
751 change of Ozone and Nitrogen oxides. Background document for the joint ÉCLAIRE/COST  
752 ES0804 Expert Workshop "From process scale to global scale: integrating our knowledge on  
753 biosphere / atmosphere exchange modelling of trace gases and volatile aerosols", 2012.](#)
- 754 Gut, A., Scheibe, M., Rottenberger, S., Rummel, U., Welling, M., Ammann, C., Kirkman, G.  
755 A., Kuhn, U., Meixner, F. X., Kesselmeier, J., Lehmann, B. E., Schmidt, W., Muller, E., and  
756 Piedade, M. T. F.: Exchange fluxes of NO<sub>2</sub> and O<sub>3</sub> at soil and leaf surfaces in an Amazonian  
757 rain forest, *Journal of Geophysical Research-Atmospheres*, 107, LBA 27-21-LBA 27-15,  
758 DOI: 10.1029/2001JD000654, 2002.
- 759 Hänsel, H., and Neumann, W.: *Physik*, Spectrum, Akad. Verl., Heidelberg, Berlin, Oxford,  
760 1995.

761 [Heal, M. R., Booth, B. B. B., Cape, J. N. and Hargreaves, K. J.: The influence of simplified](#)  
762 [peroxy radical chemistry on the interpretation of NO<sub>2</sub>-NO-O<sub>3</sub> surface exchange, Atmospheric](#)  
763 [Environment 35, 1687-1696, 2001.](#)

764 Hicks, B. B., Baldocchi, D. D., Meyers, T. P., Hosker, R. P., and Matt, D. R.: A preliminary  
765 multiple resistance routine for deriving dry deposition velocities from measured quantities,  
766 Water Air Soil Poll, 36, 311-330, DOI 10.1007/Bf00229675, 1987.

767 Högström, U.: Non-dimensional wind and temperature profiles in the atmospheric surface-  
768 layer - a re-evaluation, Boundary-Layer Meteorology, 42, 55-78, DOI 10.1007/Bf00119875,  
769 1988.

770 Holzinger, R., Lee, A., Paw, K. T., and Goldstein, A. H.: Observations of oxidation products  
771 above a forest imply biogenic emissions of very reactive compounds, Atmos Chem Phys, 5,  
772 67-75, 2005.

773 IPCC: Climate Change ~~2007~~2013: the physical science basis. [Working group I Contribution](#)  
774 [contribution of working group I](#) to the ~~fourth~~ ~~fifth~~ assessment report of the Intergovernmental  
775 Panel on Climate Change, University Press, Cambridge, UK, ~~2007~~13.

776 Jacob, D. J., and Wofsy, S. C.: Budgets of reactive nitrogen, hydrocarbons, and ozone over  
777 the amazon-forest during the wet season, Journal of Geophysical Research-Atmospheres, 95,  
778 16737-16754, DOI 10.1029/Jd095id10p16737, 1990.

779 Jacobs, A. F. G., Vanboxel, J. H., and Elkilani, R. M. M.: Nighttime free-convection  
780 characteristics within a plant canopy, Boundary-Layer Meteorology, 71, 375-391, 1994.

781 Jäggi, M., Ammann, C., Neftel, A., and Fuhrer, J.: Environmental control of profiles of ozone  
782 concentration in a grassland canopy, Atmospheric Environment, 40, 5496-5507, DOI  
783 10.1016/j.atmosenv.2006.01.025, 2006.

784 Kasanko, M., Palmieri, A., and Coyette, C.: Land cover/ land use statistics, in: Agriculture  
785 and Fishery Statistics, edited by: Coyette, C., and Schenk, H., Eurostat, Luxembourg, 158,  
786 2011.

787 Kruijt, B., Malhi, Y., Lloyd, J., Norbre, A. D., Miranda, A. C., Pereira, M. G. P., Culf, A., and  
788 Grace, J.: Turbulence statistics above and within two Amazon rain forest canopies, Boundary-  
789 Layer Meteorology, 94, 297-331, 2000.

790 Kurpius, M. R., and Goldstein, A. H.: Gas-phase chemistry dominates O<sub>3</sub> loss to a forest,  
791 implying a source of aerosols and hydroxyl radicals to the atmosphere, Geophysical Research  
792 Letters, 30, DOI 10.1029/2002gl016785, 2003.

793 Lamaud, E., Loubet, B., Irvine, M., Stella, P., Personne, E., and Cellier, P.: Partitioning of  
794 ozone deposition over a developed maize crop between stomatal and non-stomatal uptakes,  
795 using eddy-covariance flux measurements and modelling, Agricultural and Forest  
796 Meteorology, 149, 1385-1396, DOI 10.1016/j.agrformet.2009.03.017, 2009.

797 Lehmann, B. E., Lehmann, M., Neftel, A., Gut, A., and Tarakanov, S. V.: Radon-220  
798 calibration of near-surface turbulent gas transport, Geophysical Research Letters, 26, 607-  
799 610, 1999.

800 Lenschow, D. H.: Reactive trace species in the boundary-layer from a micrometeorological  
801 perspective, J Meteorol Soc Jpn, 60, 472-480, 1982.

802 Lerda, M. T., Munger, L. J., and Jacob, D. J.: Atmospheric chemistry - the NO<sub>2</sub> flux  
803 conundrum, Science, 289, 2291, DOI 10.1126/science.289.5488.2291, 2000.

- 804 Mauder, M., and Foken, T.: Documentation and instruction manual of the eddy-covariance  
805 software package TK3, Arbeitsergebnisse Nr. 46, 2011.
- 806 Monsi, M., and Saeki, T.: Über den Lichtfaktor in den Pflanzengesellschaften und seine  
807 Bedeutung für die Stoffproduktion, Japanese Journal of Botany, 14, 22-52, 1953.
- 808 Monteith, J. L., and Unsworth, M. H.: Principles of environmental physics, 2nd ed., E.  
809 Arnold, London, New York, 291 pp., 1990.
- 810 [Moravek, A., Foken, T., and Trebs, I.: Application of a GC-ECD for measurements of bio-](#)  
811 [sphere-atmosphere exchange fluxes of peroxyacetyl nitrate using the relaxed eddy accumula-](#)  
812 [tion and gradient method, Atmos. Meas. Tech., 7, 2097-2119, doi:10.5194/amt-7-2097-2014,](#)  
813 [2014a.](#)
- 814 ~~Moravek, A., Foken, T., and Trebs, I.: Application of a GC-ECD for measurements of~~  
815 ~~biosphere-atmosphere exchange fluxes of peroxyacetyl nitrate using the relaxed eddy~~  
816 ~~accumulation and gradient method, Atmos. Meas. Tech. Discuss., 7, 1917-1974,~~  
817 ~~10.5194/amtd-7-1917-2014, 2014.~~
- 818 [Moravek, A., Stella, P., Foken, T., and Trebs, I.: Influence of local air pollution on the deposi-](#)  
819 [tion of peroxyacetyl nitrate to a nutrient-poor natural grassland ecosystem, Atmos. Chem.](#)  
820 [Phys. Discuss., 14, 20383-20416, doi:10.5194/acpd-14-20383-2014, 2014b.](#)
- 821 Nemitz, E., Sutton, M. A., Gut, A., San Jose, R., Husted, S., and Schjoerring, J. K.: Sources  
822 and sinks of ammonia within an oilseed rape canopy, Agricultural and Forest Meteorology,  
823 105, 385-404, 2000.
- 824 Nemitz, E., Loubet, B., Lehmann, B. E., Cellier, P., Neftel, A., Jones, S. K., Hensen, A., Ihly,  
825 B., Tarakanov, S. V., and Sutton, M. A.: Turbulence characteristics in grassland canopies and  
826 implications for tracer transport, Biogeosciences, 6, 1519-1537, 2009.
- 827 Personne, E., Loubet, B., Herrmann, B., Mattsson, M., Schjoerring, J. K., Nemitz, E., Sutton,  
828 M. A., and Cellier, P.: SURFATM-NH<sub>3</sub>: a model combining the surface energy balance and  
829 bi-directional exchanges of ammonia applied at the field scale, Biogeosciences, 6, 1371-1388,  
830 DOI 10.5194/bg-6-1371-2009, 2009.
- 831 Plake, D., and Trebs, I.: An automated system for selective and continuous measurements of  
832 vertical thoron profiles for the determination of transport times near the ground, Atmos Meas  
833 Tech, 6, 1017-1030, DOI 10.5194/amt-6-1017-2013, 2013.
- 834 Plake, D., Stella, P., Moravek, A., Mayer, J. C., Ammann, C., Held, A., and Trebs, I.:  
835 Comparison of ozone deposition measured with the dynamic chamber and the eddy  
836 covariance method, Agricultural and Forest Meteorology, submitted, 2014.
- 837 Rinne, J., Markkanen, T., Ruuskanen, T. M., Petaja, T., Keronen, P., Tang, M. J., Crowley, J.  
838 N., Rannik, U., and Vesala, T.: Effect of chemical degradation on fluxes of reactive  
839 compounds - a study with a stochastic Lagrangian transport model, Atmos Chem Phys, 12,  
840 4843-4854, DOI 10.5194/acp-12-4843-2012, 2012.
- 841 Ripley, E. A., and Redman, R. E.: Grassland, in: Vegetation and the atmosphere, edited by:  
842 Monteith, J. L., Acad. Press, London, 1976.
- 843 Rummel, U., Ammann, C., Gut, A., Meixner, F. X., and Andreae, M. O.: Eddy covariance  
844 measurements of nitric oxide flux within an Amazonian rain forest, Journal of Geophysical  
845 Research-Atmospheres, 107, DOI 10.1029/2001jd000520, 2002.

846 Rummel, U.: Turbulent exchange of ozone and nitrogen oxides between an Amazonian rain  
847 forest and the atmosphere, PhD thesis, Faculty of Biology, Chemistry and Geosciences,  
848 University of Bayreuth, Bayreuth, 246 pp., 2005.

849 Rummel, U., Ammann, C., Kirkman, G. A., Moura, M. A. L., Foken, T., Andreae, M. O., and  
850 Meixner, F. X.: Seasonal variation of ozone deposition to a tropical rain forest in southwest  
851 Amazonia, *Atmos Chem Phys*, 7, 5415-5435, 2007.

852 Seinfeld, J. H., and Pandis, S. N.: Atmospheric chemistry and physics : from air pollution to  
853 climate change, 2. ed., Wiley, Hoboken, NJ, 1203 pp., 2006.

854 Simon, E., Lehmann, B. E., Ammann, C., Ganzeveld, L., Rummel, U., Meixner, F. X., Nobre,  
855 A. D., Araujo, A., and Kesselmeier, J.: Lagrangian dispersion of Rn-222, H<sub>2</sub>O and CO<sub>2</sub> within  
856 Amazonian rain forest, *Agricultural and Forest Meteorology*, 132, 286-304, 2005.

857 Stella, P., Kortner, M., Ammann, C., Foken, T., Meixner, F. X., and Trebs, I.: Measurements  
858 of nitrogen oxides and ozone fluxes by eddy covariance at a meadow: evidence for an internal  
859 leaf resistance to NO<sub>2</sub>, *Biogeosciences*, 10, 5997-6017, DOI 10.5194/bg-10-5997-2013, 2013.

860 Suttie, J. M., Reynolds, S. G., and Batello, C.: Introduction, in: Grasslands of the world,  
861 edited by: Suttie, J. M., Reynolds, S. G., and Batello, C., FAO, Rome, 2005.

862 Swinbank, W. C.: A comparison between predictions of dimensional analysis for constant-  
863 flux layer and observations in unstable conditions, *Q J Roy Meteor Soc*, 94, 460-&, DOI  
864 10.1002/qj.49709440203, 1968.

865 Trebs, I., Bohn, B., Ammann, C., Rummel, U., Blumthaler, M., Konigstedt, R., Meixner, F.  
866 X., Fan, S., and Andreae, M. O.: Relationship between the NO<sub>2</sub> photolysis frequency and the  
867 solar global irradiance, *Atmos Meas Tech*, 2, 725-739, 2009.

868 [Trebs, I., Mayol-Bracero, O. L., Pauliquevis, T., Kuhn, U., Sander, R., Ganzeveld, L.,](#)  
869 [Meixner, F.X., Kesselmeier, J., Artaxo, P. and Andreae, M. O.: Impact of the Manaus urban](#)  
870 [plume on trace gas mixing ratios near the surface in the Amazon Basin: Implications for the](#)  
871 [NO-NO<sub>2</sub>-O<sub>3</sub> photostationary state and peroxy radical levels, \*J. Geophys. Res.\*, 117, D05307,](#)  
872 [doi:10.1029/2011JD016386, 2012.](#)

873 Trumbore, S. E., Keller, M., Wofsy, S. C., and Dacosta, J. M.: Measurements of soil and  
874 canopy exchange-rates in the Amazon rain-forest using Rn-222, *Journal of Geophysical*  
875 *Research-Atmospheres*, 95, 16865-16873, 1990.

876 van Pul, W. A. J., and Jacobs, A. F. G.: The conductance of a maize crop and the underlying  
877 soil to ozone under various environmental-conditions, *Boundary-Layer Meteorology*, 69, 83-  
878 99, 1994.

879 Warneck, P.: Chemistry of the natural atmosphere, 2nd ed., Academic Press, San Diego,  
880 California, 927 pp., 2000.

881 [Wolfe, G. M., Cantrell, C., Kim, S., Mauldin III, R. L., Karl, T., Harley, P., Turnipseed, A.,](#)  
882 [Zheng, W., Flocke, F., Apel, E. C., Hornbrook, R. S., Hall, S. R., Ullmann, K., Henry, S. B.,](#)  
883 [DiGangi, J. P., Boyle, E. S., Kaser, L., Schnitzhofer, R., Hansel, A., Graus, M., Nakashima,](#)  
884 [Y., Kajii, Y., Guenther, A., and Keutsch, F. N.: Missing per-oxy radical sources within a](#)  
885 [summertime ponderosa pine forest, \*Atmos. Chem. Phys.\*, 14, 4715-4732, doi:10.5194/acp-14-](#)  
886 [4715-2014, 2014.](#)

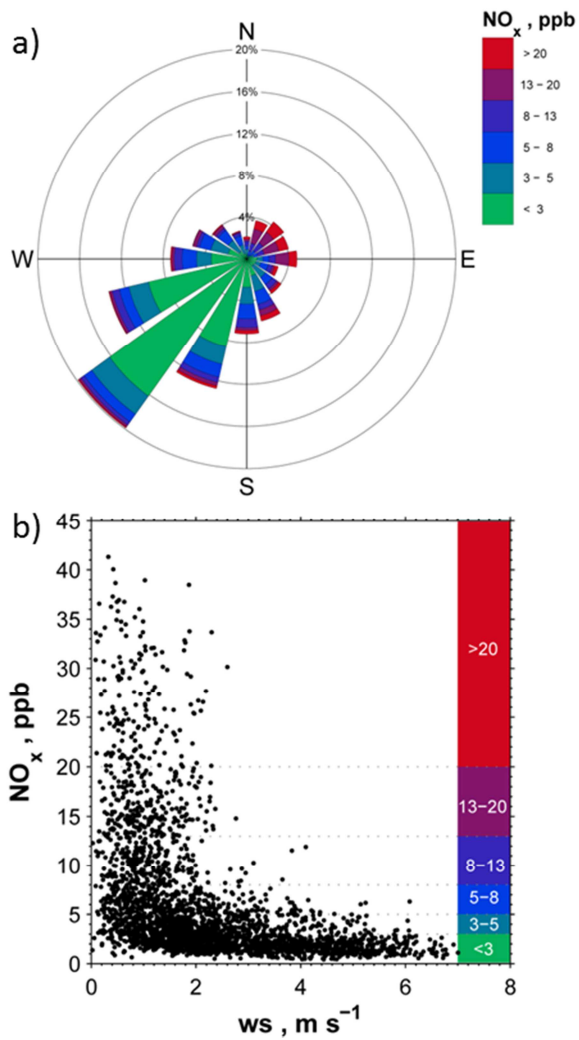
887 Yienger, J. J., and Levy, H.: Empirical-model of global soil-biogenic NO<sub>x</sub> emissions, *Journal*  
888 *of Geophysical Research-Atmospheres*, 100, 11447-11464, DOI 10.1029/95jd00370, 1995.

889

1 **Figures**

2

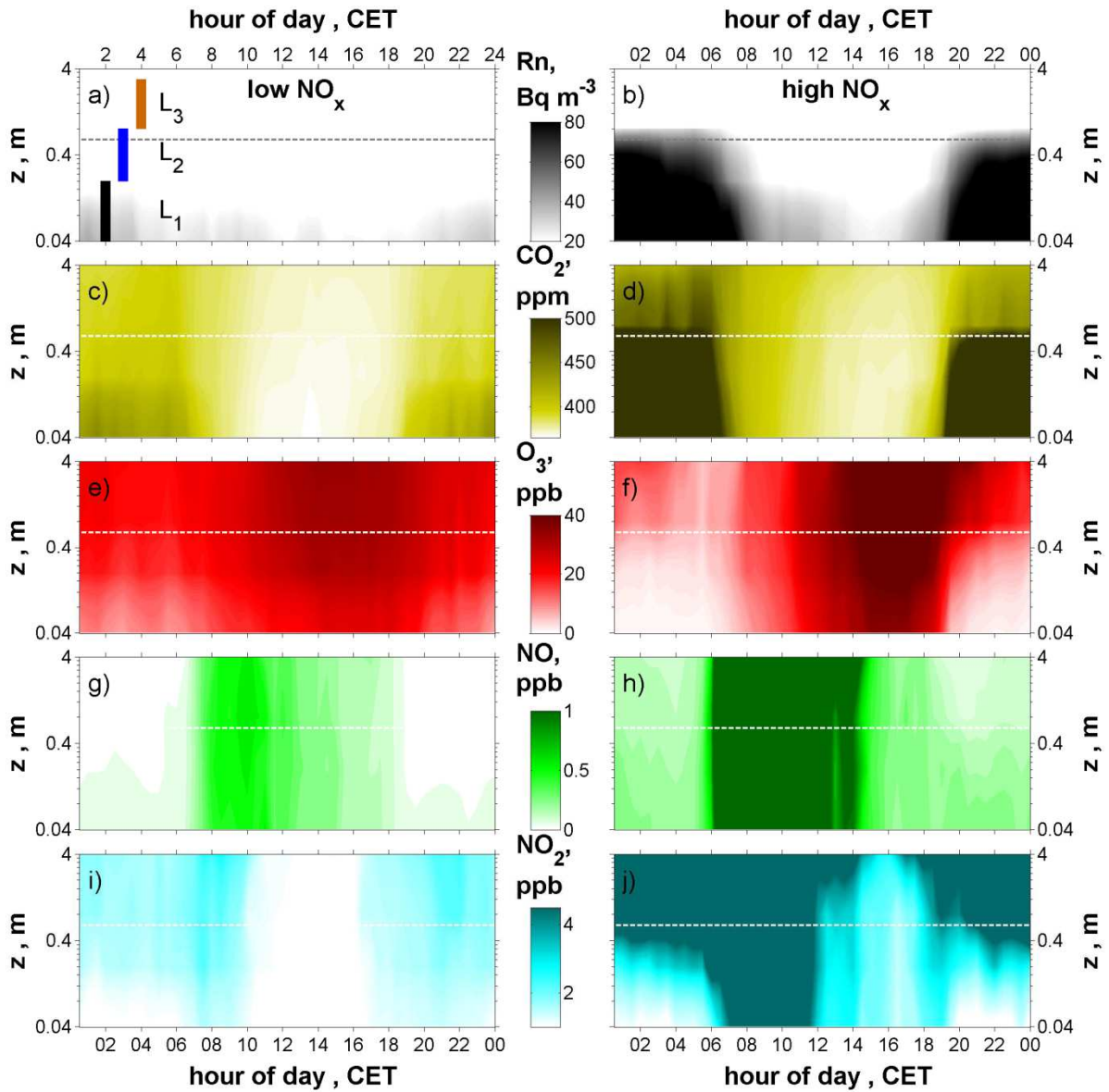
3



4

5 **Fig. 1.** (a) Frequency distribution of wind direction related to NO<sub>x</sub> mixing ratios; (b) NO<sub>x</sub>  
6 mixing ratios as function of ~~ws~~ wind speed (ws) at the Mainz-Finthen grassland site.

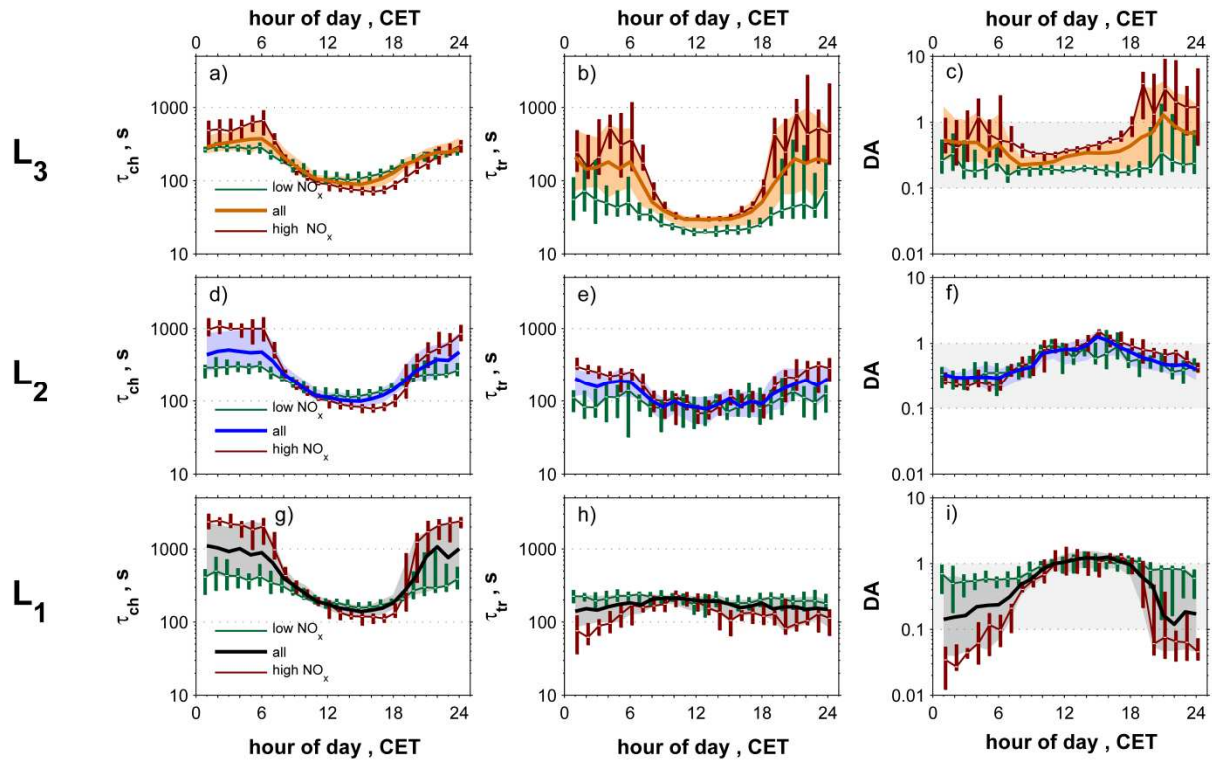
7



1

2 **Fig. 2.** Time height cross sections indicating the median vertical distribution of (a,b) Rn, (c,d)  
 3 CO<sub>2</sub>, (e,f) O<sub>3</sub>, (g,h) NO and (i,j) NO<sub>2</sub> during low NO<sub>x</sub> (left panels) and high NO<sub>x</sub> (right pan-  
 4 els) conditions at the Mainz-Finthen grassland site. The canopy height (dotted line) and L<sub>1-3</sub>  
 5 are also shown. The plots were made using the *contourf* function of MATLAB.

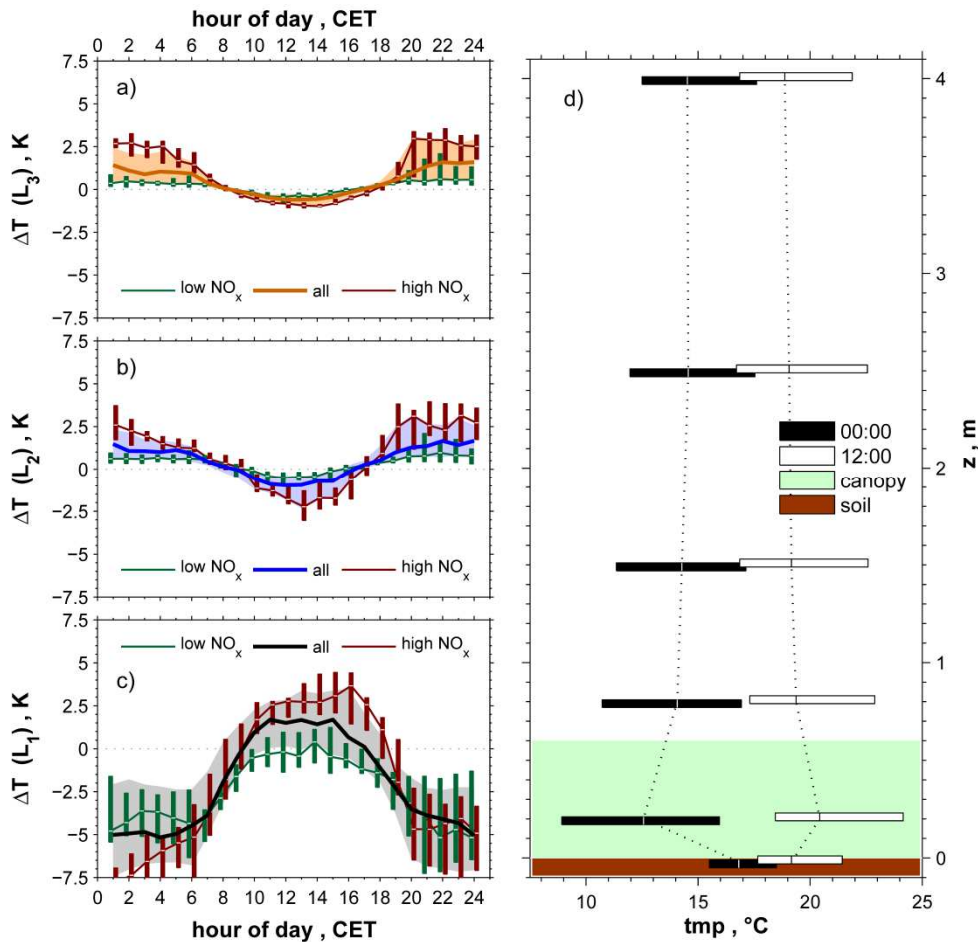
6



1

2 **Fig. 3.** Diurnal courses of (a, d, g)  $\tau_{ch}(L_{1-3})$ , (b, e, h)  $\tau_{tr}(L_{1-3})$  and (c, f, i)  $DA(L_{1-3})$  con-  
 3 sidering all data from 19 August to 26 September 2011 (medians and shaded interquartile  
 4 ranges) and the low  $\text{NO}_x$  and high  $\text{NO}_x$  periods (green and brown medians and interquartile  
 5 boxes) at the Mainz-Finthen grassland site.

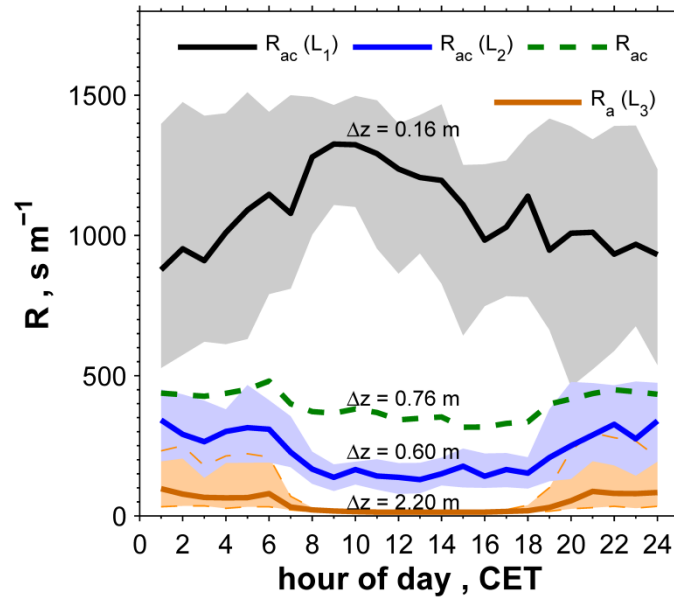
6



1

2 **Fig. 4.** (a)–(c) Diurnal courses of measured  $\Delta T(L_{1-3})$  considering all data from 19 August to  
 3 26 September 2011 (medians and shaded interquartile ranges) and the low and high NO<sub>x</sub> peri-  
 4 ods (green and brown medians and interquartile ranges); note:  $\Delta T(L_1, L_3)$  do not fully cover  
 5  $L_1$  and  $L_3$  (Sect. 2.3) due to availability of measurements (Sect. 2.2); (a)  $\Delta T(L_3)$ : 2.5 – 0.8 m;  
 6 (b)  $\Delta T(L_2)$ : 0.8 – 0.2 m; (c)  $\Delta T(L_1)$ : 0.2 – -0.02 m (soil temperature). (d) Median vertical  
 7 temperature profiles and interquartile boxes representing the thermal stratification at  
 8 00:00 and 12:00 CET considering all data from 19 August to 26 September 2011 at the  
 9 Mainz-Finthen grassland site.

10



1

2 **Fig. 5.** Diurnal courses of in-canopy aerodynamic resistances for each individual canopy layer

3  $(R_{ac}(L_1), R_{ac}(L_2))$  and for the entire grassland canopy ( $R_{ac} = \frac{\tau_{tr}(L_1) + \tau_{tr}(L_2)}{z_3 - z_1}$ ) at the Mainz-

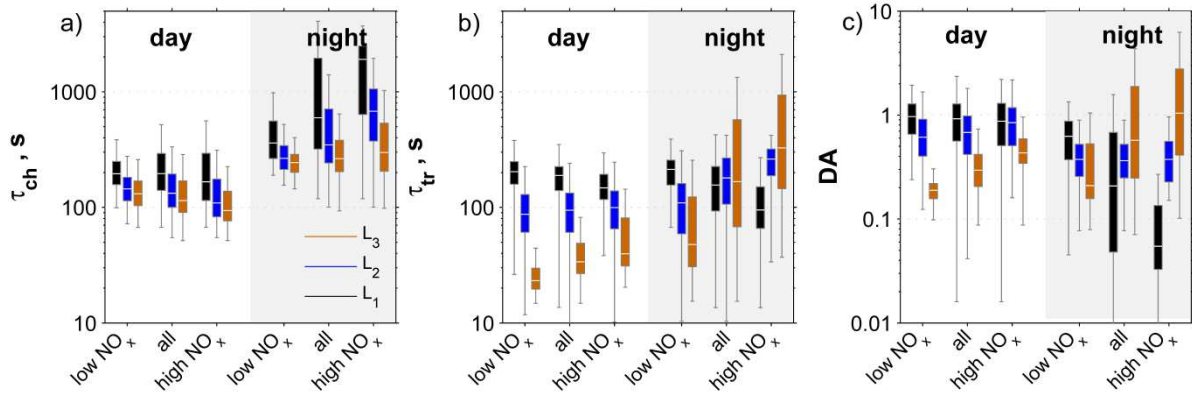
4 Finthen site (median and shaded interquartile ranges). For comparison, the aerodynamic

5 resistance above the canopy is also displayed ( $R_a(L_3)$ ). The layer thickness ( $\Delta z$ ) is indicated.

6 The plots includes all data from 19 August until 26 September 2011.

7

8

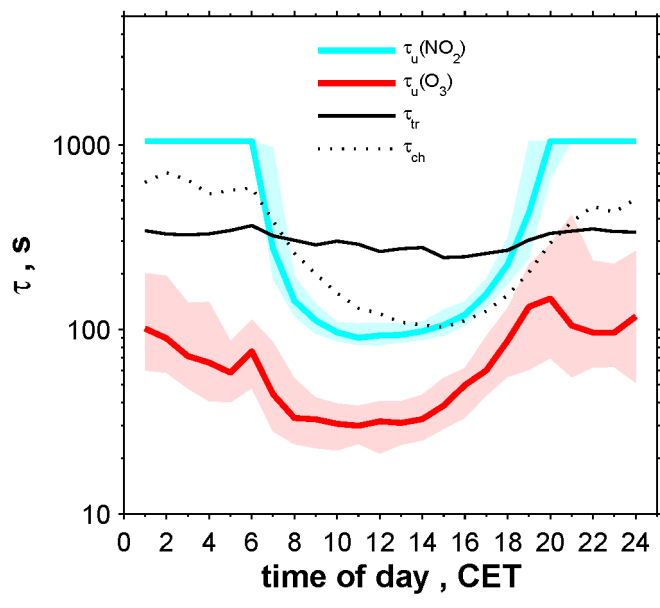


1

2 **Fig. 6.** Comparison of box plot statistics for  $\tau_{ch}(L_{1-3})$ ,  $\tau_{tr}(L_{1-3})$  and  $DA(L_{1-3})$  during day-  
 3 time and nighttime including all data from 19 August until 26 September 2011 separated for  
 4 the low and high  $NO_x$  periods at the Mainz-Finthen grassland site.

5

6

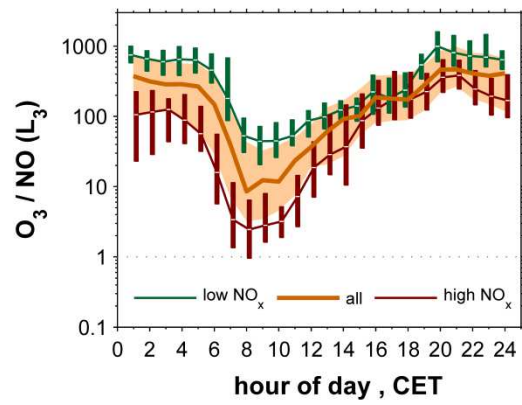


7

8 **Fig. 7.** Comparison of median diurnal  $\tau_u(NO_2)$ ,  $\tau_u(O_3)$ ,  $\tau_{tr}$  and  $\tau_{ch}$  with interquartile ranges  
 9 for the whole canopy layer ( $L_{1+2}$ ) considering all data from 19 August to 26 September 2011  
 10 at the Mainz-Finthen grassland site.

1

2

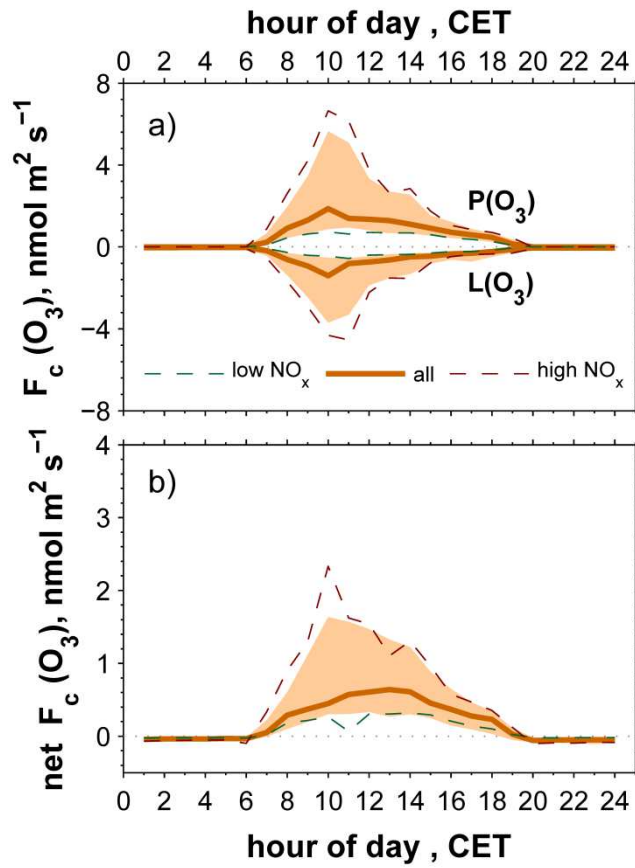


3

4 **Fig. 8.** Diurnal course of the O<sub>3</sub> to NO ratio in L<sub>3</sub> considering all data from 19 August to  
5 26 September 2011 (median and shaded interquartile range) and separated for the low NO<sub>x</sub>  
6 and high NO<sub>x</sub> periods (medians and interquartile boxes) at the Mainz-Finthen grassland site.

7

8



1

2 **Fig. 9.** Diurnal courses showing (a)  $P(\text{O}_3)$  and  $L(\text{O}_3)$  and (b)  $F_c(\text{O}_3)$  (Eq. 11) for  $L_3$  consider-  
 3 ing all days from 19 August to 26 September 2011 (medians and shaded interquartile ranges)  
 4 and separated for the low and high  $\text{NO}_x$  periods (medians) at the Mainz-Finthen grassland  
 5 site.